Nordic nuclear safety research

NKS-440
ISBN 978-87-7893-532-8

Scenarios and Phenomena Affecting Risk of Containment Failure and Release Characteristics

Weimin Ma[1], Peng Yu[1], Yangli Chen[1], Sachin Thakre[1]
Yan Xiang[1], Qiang Guo[1], Yucheng Deng[1]
Andrei Komlev[1], Walter Villanueva[1]
Sevostian Bechta[1]

Tuomo Sevón[2], Sara Ojalehto[2], Anna Korpinen[2]

[1]Royal Institute of Technology (KTH), Sweden

[2]Technical Research Centre of Finland Ltd (VTT)

July 2020

Abstract

The objectives of the project "Scenarios and Phenomena Affecting Risk of Containment Failure and Release Characteristics", dubbed SPARC, is to produce new data as well as to develop models and methodologies for addressing severe accident scenarios and phenomena which are important to assess the risk of containment failure and radioactivity release in postulated severe accidents of Nordic nuclear power plants.

In 2019 substantial advances and achievements in experimental and analytical capabilities as well new insights into physical mechanisms were gained at KTH and at VTT for: (i) experimental development and analysis of melt pool heat transfer; (ii) modeling and analysis of ex-vessel debris bed coolability; (iii) experimental study on melt coolant interaction and debris formation using metallic melt; (iv) development of a parametric code for estimating melt pool heat transfer and its application in vessel failure analysis; (v) experimental study on oxidation of metallic droplets; (vi) investigation of the effect of seawater on quenching of a hot sphere; (vii) analysis of the Fukushima accident using the MELCOR code; and (viii) CFD analyses of heat transfer in a melt pool with OpenFOAM.

This report summarizes the main advancements and findings. More details can be found in the relevant publications as listed in References.

Key words

Severe accident, melt pool heat transfer, debris coolability, fuel coolant interaction, MELCOR simulation.

NKS-440
ISBN 978-87-7893-532-8
Electronic report, July 2020
NKS Secretariat
P.O. Box 49
DK - 4000 Roskilde, Denmark
Phone +45 4677 4041
www.nks.org
e-mail nks@nks.org

Scenarios and Phenomena Affecting Risk of Containment Failure and Release Characteristics

Final Report from the NKS-R SPARC activity (Contract: AFT/NKS-R(19)122/4)

Weimin Ma[1], Peng Yu[1], Yangli Chen[1], Sachin Thakre[1], Yan Xiang[1], Qiang Guo[1], Yucheng Deng[1], Andrei Komlev[1], Walter Villanueva[1], Sevostian Bechta[1],
Tuomo Sevón[2], Sara Ojalehto[2], Anna Korpinen[2]

[1]Royal Institute of Technology (KTH)
[2]Technical Research Centre of Finland Ltd (VTT)

Executive Summary

The objectives of the project “Scenarios and Phenomena Affecting Risk of Containment Failure and Release Characteristics”, dubbed SPARC, is to produce new data as well as to develop models and methodologies for addressing severe accident scenarios and phenomena which are important to assess the risk of containment failure and radioactivity release in postulated severe accidents of Nordic nuclear power plants.

In 2019 substantial advances and achievements in experimental and analytical capabilities as well new insights into physical mechanisms were gained at KTH and at VTT for: (i) experimental development and analysis of melt pool heat transfer; (ii) modeling and analysis of ex-vessel debris bed coolability; (iii) experimental study on melt coolant interaction and debris formation using metallic melt; (iv) development of a parametric code for estimating melt pool heat transfer and its application in vessel failure analysis; (v) experimental study on oxidation of metallic droplets; (vi) investigation of the effect of seawater on quenching of a hot sphere; (vii) analysis of the Fukushima accident using the MELCOR code; and (viii) CFD analyses of heat transfer in a melt pool with OpenFOAM.

This report summarizes the main advancements and findings. More details can be found in the relevant publications listed in References.

Table of contents

1. Introduction

The goal of this project is to produce new data, and to develop models and methodologies for addressing severe accident scenarios and phenomena which are important to assess the risk of containment failure and radioactivity release in a postulated severe accident of Nordic nuclear power plants. The experimental studies and deterministic modelling at KTH and at VTT provide necessary insights and data for definition of severe accident scenarios and development of tools which are important for safety analysis. Therefore, this joint research project enables the two Nordic partners to leverage their ongoing projects, so as to maximize the research outcomes and spread the excellence to each other. The collaborative project also helps establish/enhance the informal Nordic networks for information exchange on severe accident research.

Leveraging on the ongoing research activities of KTH and VTT in the respective APRI-10 and SAFIR2022 Programmes, the work packages and tasks of the SPARC project in 2019 were conceived as follows to focus on deterministic investigations on severe accident.

WP1: <u>Experimental study of severe accident phenomena and modeling development</u> for assessment of core melt risk and corium stabilization in a Nordic BWR.

1.1 ***In-vessel debris/molten pool behavior and RPV failure***, in order to gain insights into complex in-vessel phenomena, including remelting of a debris bed to a molten pool, heat and mass transfer to the vessel wall and penetrations, failure of RPV penetrations (e.g., CRGTs – Control Rod Guide Tubes, IGTs – Instrument Guide Tubes), and melt release scenarios including breach ablation/clogging issues.

1.2 ***Ex-vessel debris bed coolability***, in order to produce new data to address the following critical issues: post dry-out heat and mass transfer of a debris bed, and corium oxidation and debris remelting.

1.3 ***FCI and steam explosion***, involving large and small scale experiments to study molten fuel coolant interactions (FCI), using various oxides mixture and metal compositions to address material effects on melt fragmentation, Zircaloy and steel oxidation and hydrogen generation, and triggered and spontaneous steam explosion and its suppression.

1.4 ***Modelling development for deterministic analysis***.

WP2: <u>Severe accident safety analysis for nuclear power plants</u>

2.1 ***Analysis of Fukushima accident using the MELCOR code***, in order to improve the expertise of KTH and VTT in severe accident modelling using data from a real full-scale severe accident, gain a better understanding of the events in the Fukushima reactors, get insights into the capabilities and weaknesses of the MELCOR code, and enhance networking between Finnish and Swedish severe accident experts.

2.2 ***CFD analyses of heat transfer in debris/melt pool***, in order to improve the expertise of KTH and VTT in simulation of corium behavior using mechanistic modelling (instead of lumped-parameter); transfer the experimental findings to modelling capabilities; explore the capabilities and limits of CFD codes for corium heat transfer analysis; and enhance networking between Finnish and Swedish experts for advanced simulation approaches for reactor safety analysis.

This report summarizes the progress and achievements of the project during 2019. The research activity has a synergic collaboration with the Swedish APRI-10 research program, the EU project IVMR, and the Finnish SAFIR2019 programme. The project was also co-supported by VTT own research funds.

2. Results and discussions

2.1 In-vessel debris/molten pool behavior and RPV failure

Based on the previous REMCOD experimental study at KTH on remelting phenomena of debris beds (Hotta et al., 2019), a new test facility named MRSPOD (Multicomponent Remelting, relocation, and Solidification in POrous Debris) was built in a vertical tube furnace to minimize the wall effects and have better control on the temperature inside the porous debris bed. In addition to thermocouples (TC), Testing Fiber Bragg Grating (FBG) sensors were employed to detect melt penetration front position. The tube furnace has three independent heating zones for better control of the boundary conditions. After commissioning test of the MRSPOD facility (Hoseyni et al., 2019a), the first test (E16) has been performed successfully (Hoseyni et al., 2019b), under the condition of nearly uniform temperature inside the porous debris. Other conditions were kept the same as commissioning test with axial thermal gradient. A completely different behavior was observed for melt penetration and the final shape of ingot. Melt front position were identified with the help of TC and FBG readings. Improvement of measurement techniques were finalized for future tests. More new tests are planned for future MRSPOD experimental studies to clarify the effect of wettability on the melt infiltration and solidification.

In order to address the behavior of core melt (corium) in the lower head of a light water reactor (LWR) during postulated severe accidents, the SIMECO-2 facility (Komlev et al., 2019 & 2020) is being developed at KTH for experimental studies on heat and mass transfer in a molten pool of oxidic and metallic corium simulants, as well as remelting of debris bed and molten pool formation. The main components of the facility have been manufactured and delivered to KTH, which include a slice vessel, a high-frequency induction generator with inductors, Fiber Bragg Gratings (FBG) temperature probes, each having up to 23 measurement points. The components are being assembled after separate testing. The commissioning of the facility is expected to be realized in 2020. Meanwhile, more pre-test simulations were performed (Khan et al., 2019; Bian et al., 2019).

For prediction of RPV failure during severe accidents, coupled thermo-mechanical analysis was employed to investigate the vessel creep failure; see more details below.

2.2 Analysis of ex-vessel debris bed coolability

Various studies on ex-vessel debris bed coolability have been performed at KTH with both experiments and numerical simulation. (Li et al., 2012; Ma and Dinh, 2010; Thakre et al., 2014). The MEWA module of COCOMO code has been successfully validated against experiments regarding the boiling-off and quenching behavior of particulate debris bed, and applied to the assessment of prototypical debris bed coolability (Huang & Ma, 2018a; Huang & Ma, 2018b; Huang & Ma, 2019; Huang, 2019). However, the simulation with COCOMO code is quite time-consuming and computationally expensive when large number of simulation runs will be involved, such as in the case with sensitivity and uncertainty study. Moreover, there is a clear need for a quick estimation of the coolability of a multi-dimensional debris bed in a probabilistic risk analysis (PRA). For these purposes, a research effort at KTH was devoted to develop a surrogate model to predict the dryout power density of multi-dimensional debris bed, based on database of the COCOMO calculations (full-model simulations). The surrogate model is also facilitating the coupling with system codes (e.g. MELCOR) so to extend the capabilities of system codes for postulated severe accident analysis of light water reactors.

As the first step, the multi-dimensional debris bed considered in the study is axisymmetric with homogenous particle size and porosity. The debris bed is assumed to be shaped as either a cone or a cone sitting above a cylinder (see more details in Chen & Ma, 2019). The surrogate model employs a characteristic factor to represent the multi-dimensionality of the debris bed. It is defined as the dryout power density of the multi-dimensional debris bed (calculated by the COCOMO code) divided by the dryout power density of the corresponding one-dimensional debris bed with the same bed height (calculated by Lipinski 0-D model). Input parameters for the surrogate model are identified in regards to debris bed properties and pool condition, which include debris bed porosity, effective particle diameter, total debris mass, slope angle, cavity radius and pool ambient pressure. Samples are generated within the whole variation limits of each parameter and simulated with the COCOMO code to calculate the dryout power density as the full-model prediction. Based on the samples, the surrogate model is successfully developed with Kriging method, and the validation demonstrates that the model error is within $\pm 10\%$.

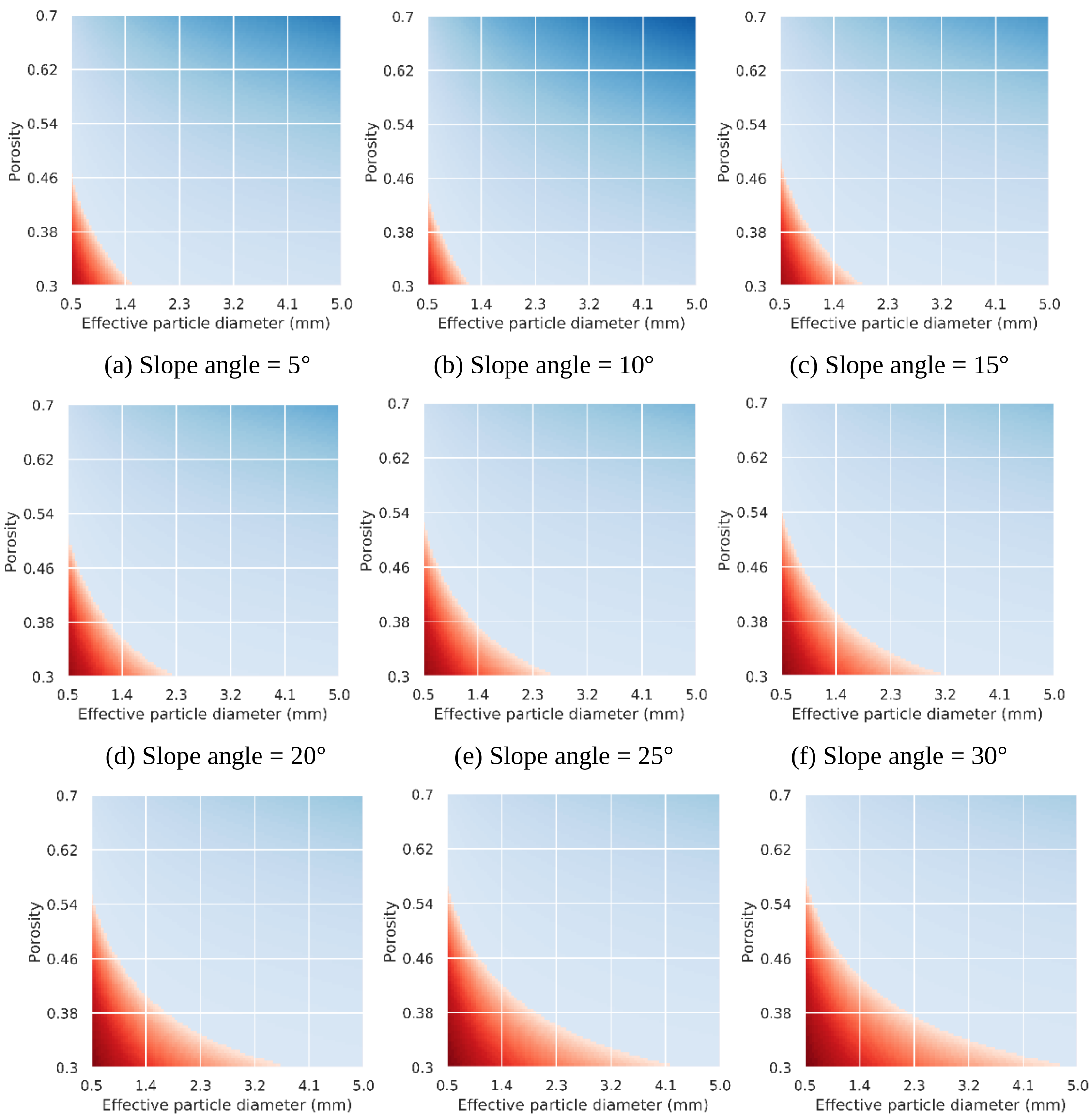

(a) Slope angle = 5°   (b) Slope angle = 10°   (c) Slope angle = 15°

(d) Slope angle = 20°   (e) Slope angle = 25°   (f) Slope angle = 30°

(g) Slope angle = 35°   (h) Slope angle = 40°   (i) Slope angle = 45°

Figure 1: Coolability maps with the variations of porosity and particle size at different slope angle.

The sensitivity study on the input parameters show that three of the parameters, including pressure, particle diameter and porosity, show positive linear relationship with the dryout power density, which means higher values of pressure, porosity, and particle size promote the debris bed coolability. Slope angle, bed mass show negative linear relationship. Because higher values of slope angle and bed mass lead to longer cooling path inside debris bed for the coolant, and therefore decrease the coolability. Large radius of the reactor cavity allows smaller slope angle, thus promotes the coolability, but it has the least influence.

As an application of this surrogate model, the coolability of ex-vessel debris bed is analyzed for a reference Nordic BWR. The coolability maps regarding the variation of porosity and particle size of the prototypical debris bed are shown in Figure 1, with different slope angles. For each coolability map, 100 × 100 samples are used. The red color roughly illustrates the non-coolable domain in regard with the variation of porosity and effective particle diameter. Small values of porosity and effective particle size would lead to non-coolable condition. The area with red color increases with the increase of slope angle, meaning that there is more chance to have non-coolable debris bed if larger slope angle is observed.

2.3 Debris bed formation using metallic melt

Previously, the DEFOR experiments (Karbojian et al., 2009; Kudinov et al., 2010) using melt of binary oxides were carried out at KTH to identify the characteristics of debris bed formed from fuel coolant interactions, which are of importance to debris bed coolability. DEFOR experiments using melt of binary oxides were carried out to identify the characteristics of a debris bed formed from fuel coolant interactions), which influence debris bed coolability. The morphology and size distribution of the debris particles of DEFOR is similar to those of other experiments using prototypical materials (Spencer et al., 1994; Magallon et al., 1999; Magallon & Huhtiniemi, 2001), with the porosity of 40%~60% for debris beds. However, more and more evidence indicated that the first pour of corium upon vessel failure is most likely to be a metal rich jet. Therefore, an experimental study on metallic melt-coolant interactions and oxidation was initiated at KTH in 2018. The DEFOR facility has been adopted to investigate fuel coolant interactions (FCI) using molten Tin, with the objective to look into the characteristics of metallic debris beds formed from FCI.

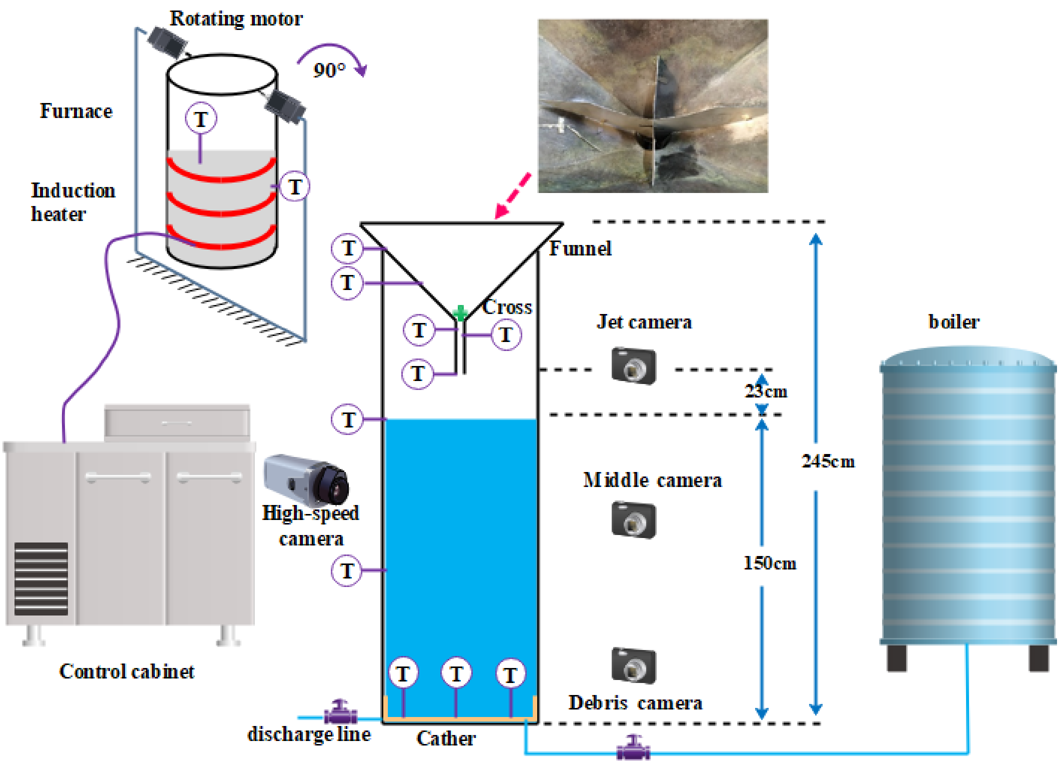

Figure 2: DEFOR-M schematic campaign.

The schematic of the new test facility (named DEFOR-M) is as shown in Figure 2. A series of experiments with the test matrix in Table 1 have been conducted using the metallic melt, Tin, in order to study the melt jet fragmentation, jet break up, debris formation (geometrical shape and porosity), particles morphology and size distribution. Effect of melt superheat and water subcooling on the above-mentioned parameters and factors were also studied.

Table 1: Test matrix or DEFOR-M

Parameters	H-L	M-L	L-L	M-H	M-M
Simulant material	Sn				
Melt density [kg/l]	7.310				
Melting temperature [℃]	231.93				
Melt temperature in the funnel [℃]	346	314	282	309	307
Melt superheat in the funnel [℃]	115	82	50	77	75
Melt jet initial diameter [mm]	20				
Elevation of nozzle outlet [m]	1.7				
Jet free fall height [m]	0.23				
Duration of melt release [s]	8.3	7.45	7.32	7.3	7.16
Melt volume [l]	4.1				
Average flow rate [l/s]	0.494	0.55	0.56	0.56	0.57
Water pool depth [m]	1.5				
Water initial temperature [℃]	98	90	90	50	70
Water subcooling [℃]	2	10	10	50	30
Debris collection [kg]	29.706	29.138	29.356	29.45	29.76
Agglomeration[kg]	25.7	-	-	-	-

2.3.1 Jet breakup length

There are various methods to estimate the melt jet breakup length in a water pool, which is a challenging task especially in the presence of vapors. In the present study (Thakre et al., 2019), two methods are used.

In the first method, an intersection point of the extended cone of the jet spread with the extended jet diameter is considered at the jet breakup location (**Error! Reference source not found.** 3a). W hereas, in second method, a jet breakup is interpreted at the location where the velocity of the jet front start to decrease (**Error! Reference source not found.** 3b). These methods are implemented according to the observations, where the melt jet form an extended cone near the expected breakup zone. In addition to that, the velocity of the continuous jet front start to decrease after the jet breakup and saturate thereafter. The jet breakup length data is containing ± 15% uncertainty in both the methods. The jet breakup length data is then compared with the existing experimental data and some widely used breakup models. Figure 4 shows the jet breakup length is closely estimated by the Saito's correlations and lies between Taylor's correlation and Matsuo's correlation.

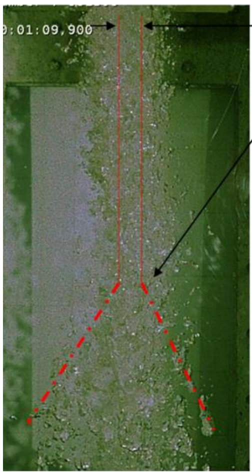

$L_{(breakup)}$ (m) Method 1	$L_{(breakup)}$ (m) Method 2
0.53	0.485 (±0.7)
0.51	0.49 (±0.6)
0.53	0.475 (±0.7)

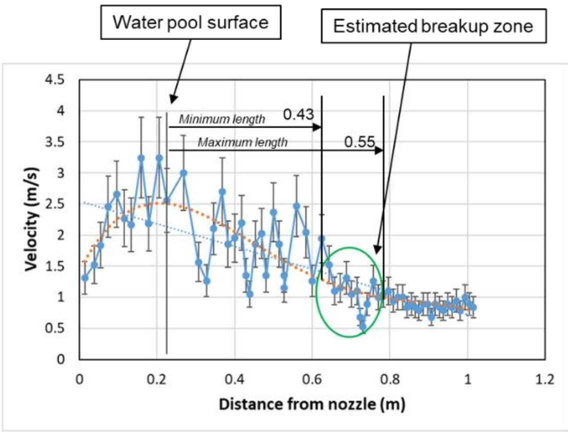

a) method 1 b) method 2

Figure 3: Jet breakup estimation using two methods.

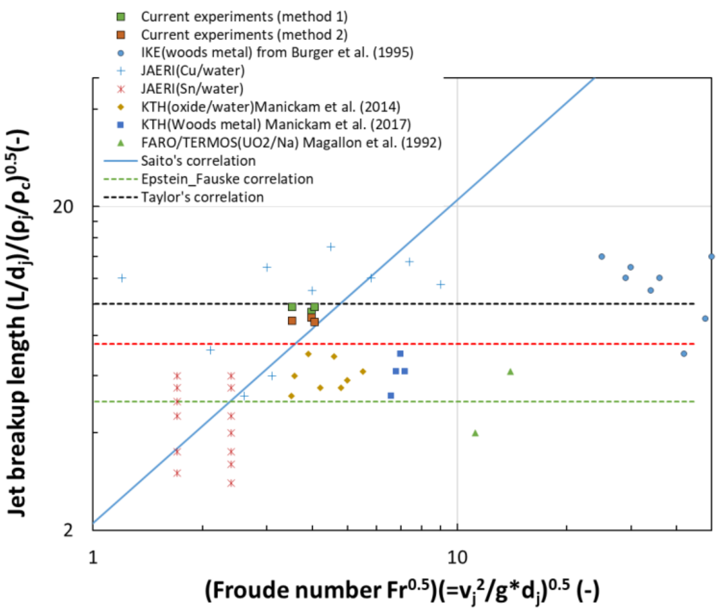

Figure 4: Jet breakup length comparison with other experimental data and models.

2.3.2 Debris characteristics

After the fragmentation of the melt jet in the water pool, the resulting debris particles will be quenched and settle on the floor of the water tank, forming a debris bed. The characteristics of the debris bed are analyzed in the present study (Xiang et al., 2019).

Figure 5 shows the evolution of a debris bed forming from the melt-coolant interaction test L-L (low superheat of melt and low subcooling of coolant), where time zero is set as the point when the melt is discharged from the nozzle outlet. The travelling period of the jet leading edge from the nozzle outlet to the water tank bottom is 1.88s, which means that the average velocity of the initial phase is about 0.92m/s.

Solid Tin particles are found as it arrived at the bottom without further generation of steam bubbles, indicating the debris particles were fully quenched and cooled down for the first pour. Scattered particles are located on the bottom and spreading out to the periphery. Resulting from fine fragmentation and intense mixing, debris particles show a variety in size distribution and reach the side walls at 2.28s. As the coherent melt jet is penetrating through the water pool, steam bubbles are generated around the central line, forming a cloud of mixture of melt droplets and steam bubbles (see the snapshot at 2.76s). Steam bubbles are also generated and rise at the sides, leading to a clear recirculation pattern at 3.56s. This is because some debris particles of the later discharged melt remain high temperature (over saturated temperature of water) at their arrival at the bottom due to insufficient cooling.

Later, a conical debris bed is formed at the bottom and covered with a thick layer of steam bubbles. Following the generation of large amount of steam bubbles, the clear recirculation disappears, and the bubbles flow upward to fill in the water tank at 4.45s. Strong evaporation continues until the end of melt discharge. The final debris bed was formed at 9.75s, which has almost the same conical angle of that at 3.56s.

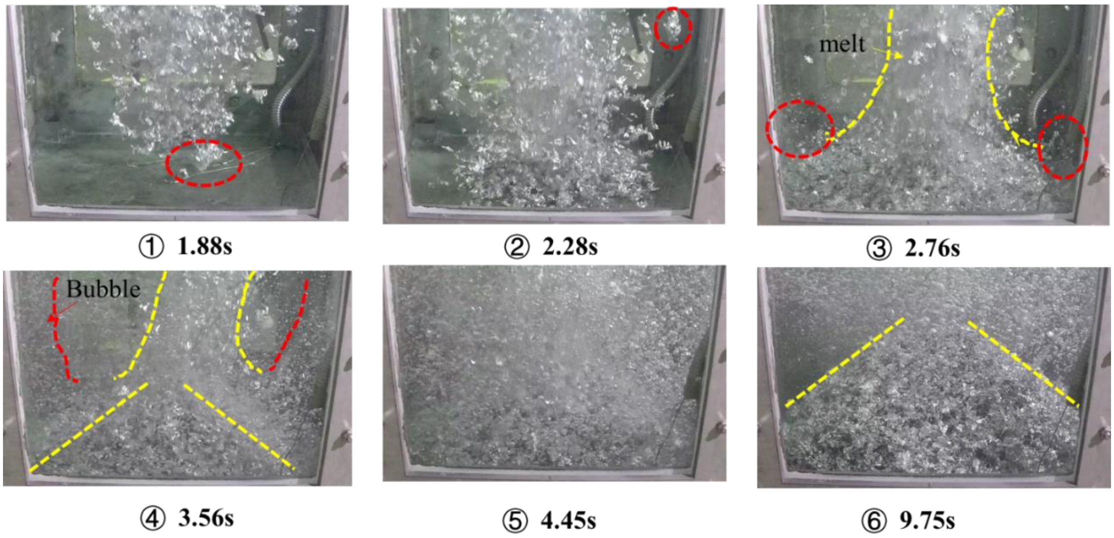

Figure 5: Snapshots of the debris bed formation process.

The debris beds of the three tests L-L, M-L and H-L (around 30kg each) are shown in Table 2. They are all conically shaped, and agglomeration of debris particles is observed in the H-L case. The debris beds in the M-L and L-L cases show inhomogeneity and stratification in particle sizes, with smaller particles tending to settle at the bottom while the larger ones at the top, which was also found in the DEFOR-E tests using oxidic melt (Karbojian et al., 2009).

The particles in the peripheral region was driven by coolant flow as well as fine fragmentation. The melt superheat has a significant influence on the morphology of debris particles. Smooth and round particles are found at high superheat while porous and flat particles are formed at low superheat. This is because in the high superheat case, the fragmented particles remain liquid droplets with surrounding film boiling for a relatively longer time during their falling in the water pool, which provides a favorable condition and time scale for surface tension to play an important role in solidification, resulting in the smooth and round particles. On the contrary, for the low melt superheat case, since the debris particles are rapidly solidified and quenched during their travelling in the water pool, the thermal stress and impact of vapor film collapse may all contribute to fragmentation of debris. The wire-like particles are observed due to ductility of metallic melt, which are quite different from the morphology of particles of oxidic melt.

Figure 6 shows the particle size distributions for different tests. It can be found that lower melt superheat gives rise to larger debris particles by average.

Table 2: Debris bed comparison

Case	Debris bed	Cross section	Particle morphology
H-L $\Delta T_m = 114$℃			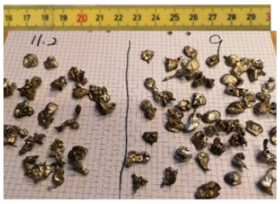
M-L $\Delta T_m = 82$℃			
L-L $\Delta T_m = 50$℃	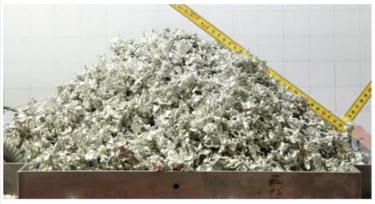		

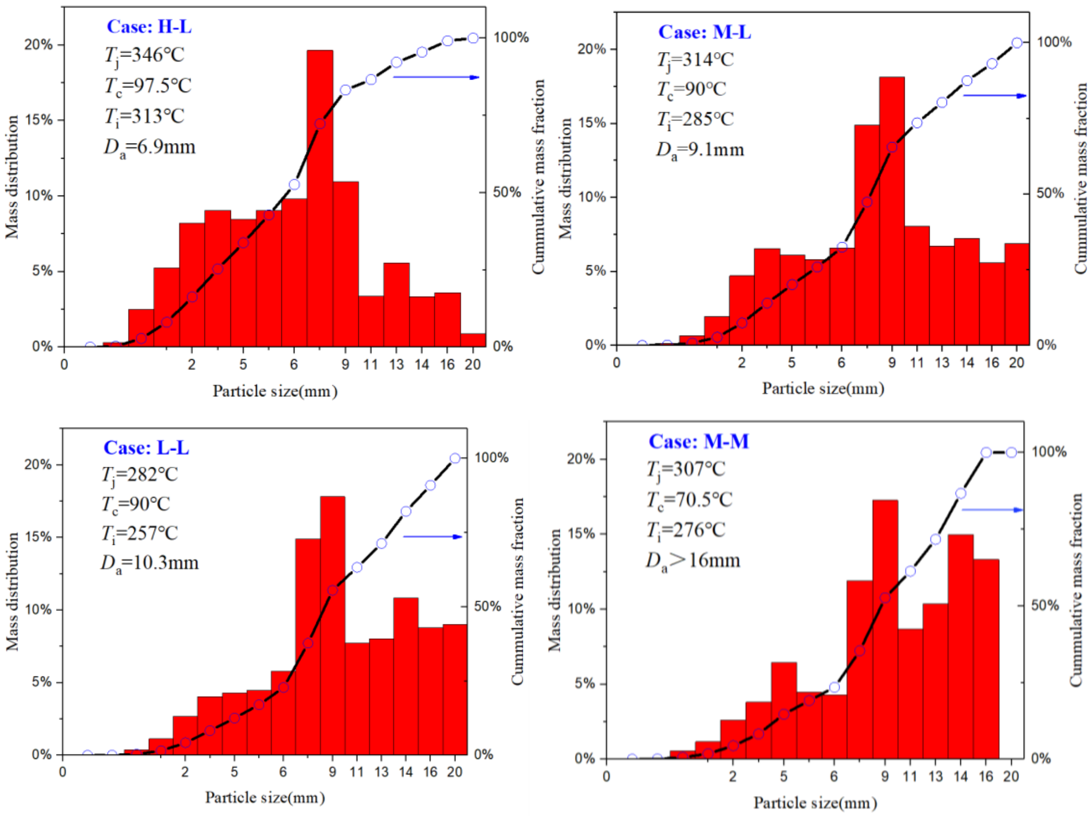

Figure 6: Particle size distributions.

There are several thermodynamic fragmentation models using interface instability theories, including Kelvin–Helmholtz (K-H) instability, Rayleigh–Taylor (R-T) instability and critical Weber number criteria (Abe et al., 2004), which can be employed to estimate the average particle size, if the critical wavelength of these theories is assumed to equal the debris size. For

K-H instability theory, the minimum unstable wavelength can be proposed as the relative velocity determined at the interface:

$$\lambda_{K-H} = \frac{2\pi\sigma_j(\rho_j + \rho_s)}{u^2\rho_j\rho_s} \quad (1)$$

The minimum wavelength based on Rayleigh–Taylor instability can be yielded at the fastest growth rate:

$$\lambda_{R-T} = 2\pi\sqrt{\frac{3\sigma_j}{(\rho_j - \rho)g}} \quad (2)$$

The critical Weber number criteria is based on the balance between surface tension and shearing force. For turbulent flow, the most stable size can be expressed as:

$$d = \frac{18\sigma_j}{u^2\rho_s} \quad (3)$$

where σ_j is the surface tension of melt, ρ_s the density of surroundings, u the relative velocity of melt and surroundings.

The comparison of the experimental data with the three instability theories is shown in Figure 7 as the surrounding fluid is steam or water. The steam velocity can be set as 32m/s based on the experiment of Pohlner (Pohlner et al., 2006). If the critical size of instability theories are assumed to equal the median size of the debris particles in the debris beds, it can be seen that the size predicted by the K-H instability with surrounding steam is in the range of obtained particle size in the DEFOR-M tests, but the critical size is quite small if water is considered as surrounding fluid. The R-T instability generally overestimates the median size no matter what the surrounding fluid is. The critical Weber number criteria depends on the surrounding fluid for the size prediction. Therefore, in the range of this test condition, jet fragmentation is mainly driven by the counter-current flow of melt and vapor around. The K-H instability dominates the fragmentation behavior, causing crust stripping off and porous debris formation.

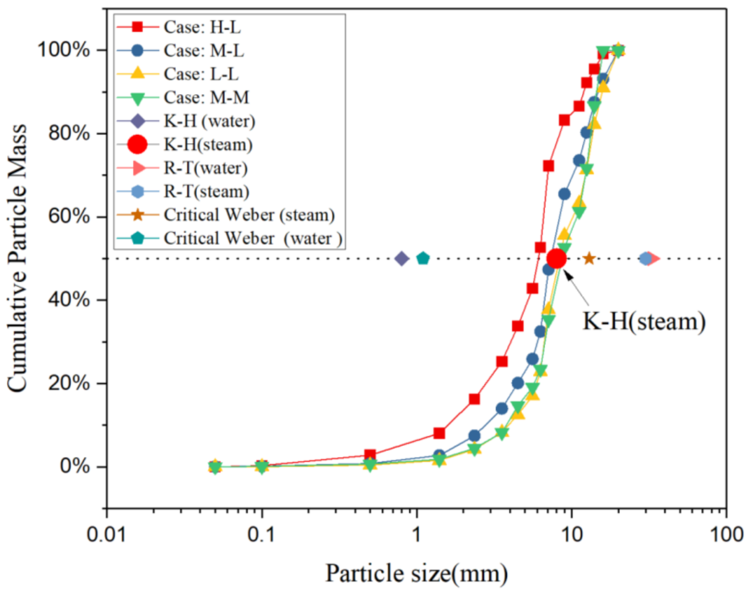

Figure 7: Comparison with existing theories.

2.4 Parametric modelling of transient melt pool heat transfer

In the late phase of in-vessel progression during a hypothetical severe accident, a melt pool may form in the lower head, imposing significant thermal loads on the reactor pressure vessel (RPV). If the cooling of the melt pool can not sufficiently remove the decay heat, the RPV would fail due to creep under the thermal attack of the melt. The prediction of the vessel failure is a coupled problem of thermal-mechanical simulations per se, i.e. both the melt pool heat transfer and the vessel wall mechanical behavior need to be modeled.

Traditionally the melt pool heat transfer can be stimulated by CFD (e.g. turbulence modeling, and then coupled with analysis of structural mechanics, so as to obtain the location and timing of vessel failure (Yu et al., 2019), However, such mechanistic approach of melt pool convection simulation is computationally expensive for a prototypical melt pool with high turbulence at large Rayleigh number. To overcome this limit, a parametric code (named 'transIVR') was developed in the present study. The transIVR code is not only capable of quick estimate of transient heat transfer of one and two- layer melt pool, but also solving heat conduction problem in the RPV wall with 2D finite difference method to provide spatial thermal details for RPV structural analysis. The code employs empirical correlations of heat transfer coefficients (from experiments) to determine global and local heat transfer, and consider energy balances in oxide layer, the metal layer and the RPV wall (Yu, 2020).

The UCSB FIBS benchmark case (Theofanous et al., 1996) was calculated to demonstrate the capability of the transIVR code in simulating two-layer melt pool (steady-state) heat transfer problems. In addition, for the code to calculate transient melt pool heat transfer, the LIVE-7V experiment (Miassoedov et al., 2014) was also considered in the validation. The experiment employed the LIVE-3D hemispherical facility with an inner diameter of 1 m . The non-eutectic binary salt mixture of 20 mol% $NaNO_3$- 80 mol% KNO_3 was used as the simulant material of corium melt. Water cooling was applied to the top and vessel surfaces. The transient process was realized by changing the heating power from 29 *kW* to 24 *kW*, then to 18 *kW* and finally to 9 *kW* along time.

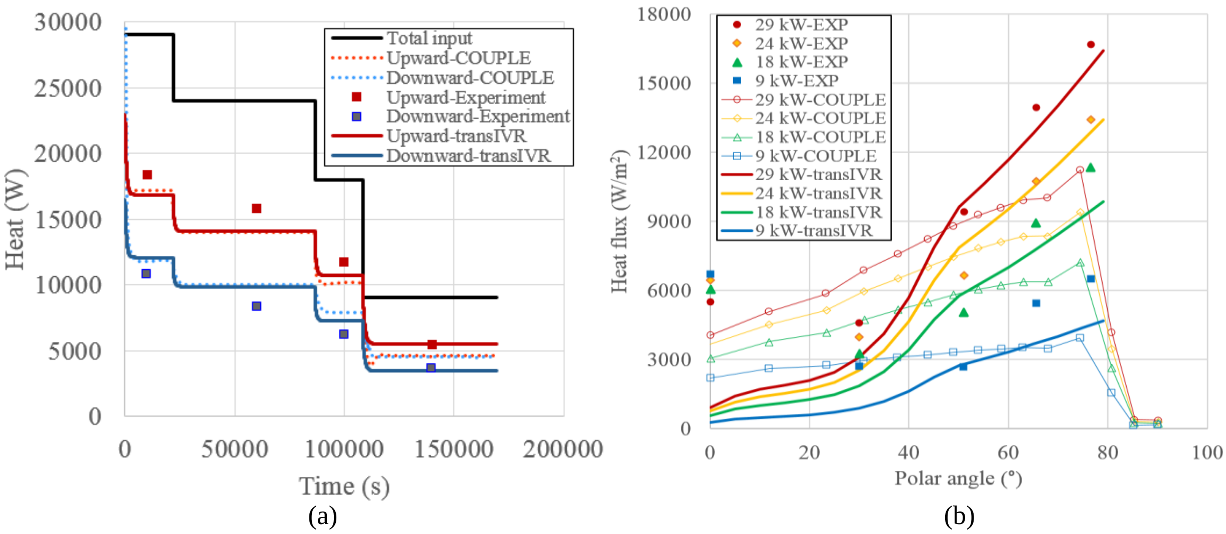

Figure 8: Simulation results of LIVE-7V experiment - (a) energy split and (b) heat flux distribution.

Figure 8 shows the transIVR simulation results in comparison with those of the experiment and the RELAP/SCDAP simulation (labelled 'COUPLE') from (Madokoro et al., 2018). Figure 8a shows the comparison of heat removal upward to the top lid and downward to the bottom vessel surface. The black curve indicates the total input power that was changed with time from 29 *kW* to 24 *kW*, 18 *kW* and 9 *kW*. For the first three stages, the transIVR predictions agree well with the COUPLE predictions, though the upward heat was underestimated compared with the experiment. For the last stage with 9 *kW* input, the transIVR agrees well with the experimental data while the COUPLE predicted an equal split between upward and downward heat loads. Figure 8b shows the comparison of the heat flux distributions along the vessel wall. For all the results, the heat flux profile gradually decreases as the total input decreases from 29 *kW* to 24 *kW*, 18 *kW* and 9 *kW*. Compared with the COUPLE results which had relatively flat distribution, the transIVR predictions generally agree better with the experimental data.

2.5 Coupled thermal-mechanical analysis of vessel failure

In this study, the transIVR code was coupled to the mechanical solver ANSYS Mechanical for detailed RPV failure analysis, and then employed to simulate the FOREVER-EC2 experiment (Theerthan at al., 2001) with the objective to validate the performance of the coupled approach for RPV failure analysis. The FOREVER-EC2 experiment is one of the FOREVER experiments that were carried at KTH to investigate vessel creep failure under thermal attack of a melt pool. The test section is a 1:10 scale of a reactor pressure vessel with a wall thickness of 15 mm. The lower head was made of 16MND5 steel. The binary mixture of 30% CaO- 70% B_2O_3 was employed as simulant of corium. A specially designed heater was immerged in the melt pool to generate the internal heat which corresponds to the nuclear decay heat. The power input was maintained ~38 kW during the experiment such that maximum melt pool temperature would be ~1300 °C. The pressure inside the vessel was maintained at 2.5 MPa

Figure 9 shows some simulation results compared with those of our previous analysis using CFD for pool heat transfer (Yu et al., 2019) and experimental measurements.

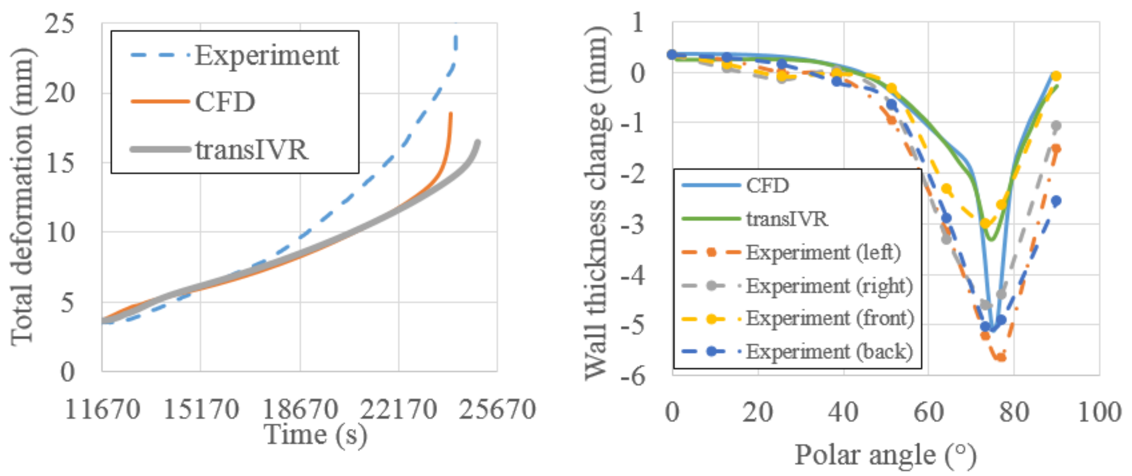

Figure 9: Simulation of FOREVER-EC2 experiment - (a) total deformation of vessel bottom and (b) wall thickness change.

Figure 9a is the total deformation of the vessel bottom in the vertical direction. The result predicted by the new coupled approach using the transIVR code was in a reasonable agreement with the experimental and CFD-related data: all three curves increase gradually with time at the beginning and experience drastic accelerations at the end. The times of vessel deformation acceleration for are 24180s, 23959s and 24959s for experiment, CFD and transIVR, respectively. Figure 9b is the comparison on wall thickness change at vessel failure time. The transIVR simulation result fits the experimental and CFD data well in the region 0°~50°. In the upper region 50°~90°, wall thickness gradually decreases with angle till around 75° and then increases till 90°. The maximum thickness change occurred at around 75°, with the value of -3 mm for the transIVR simulation, which is close to the measured of the left-side sensor in the experiment but slightly larger than those of the other sides and the CFD simulation. Considering the uncertainties in modelling approximation and numerical setting, it can be concluded that the new coupling framework successfully captured the vessel creep failure characteristics while having computational efficiency. More details can be found in (Yu, 2020).

2.6 MISTEE experiment on oxidation of metallic droplets

During a hypothetical severe accident of light water reactors, the molten reactor core (corium) may fall into a water pool, leading to fuel coolant interactions (FCI). Due to the existence of metallic components (e.g. Zr, Fe) in the corium, oxidation reaction of the metallic phases with coolant may occur, releasing reaction heat and hydrogen which all affect accident progression and severity (e.g. the reaction heat may prolong the liquid state of corium, while the non-condensable hydrogen could reduce the explosivity of corium but increase loads of potential explosion and create a combustible atmosphere). Motivated by this interest, an experimental study on the MISTEE facility at KTH (Figure 10) was carried out to investigate the hydrogen production and oxidation degree of molten metallic droplets falling into a water pool. The droplet is levitated by argon gas in the crucible (Guo et al., 2019a) during its melting and heat-up, and then discharged into the water pool by switching the three-way valve to "open".

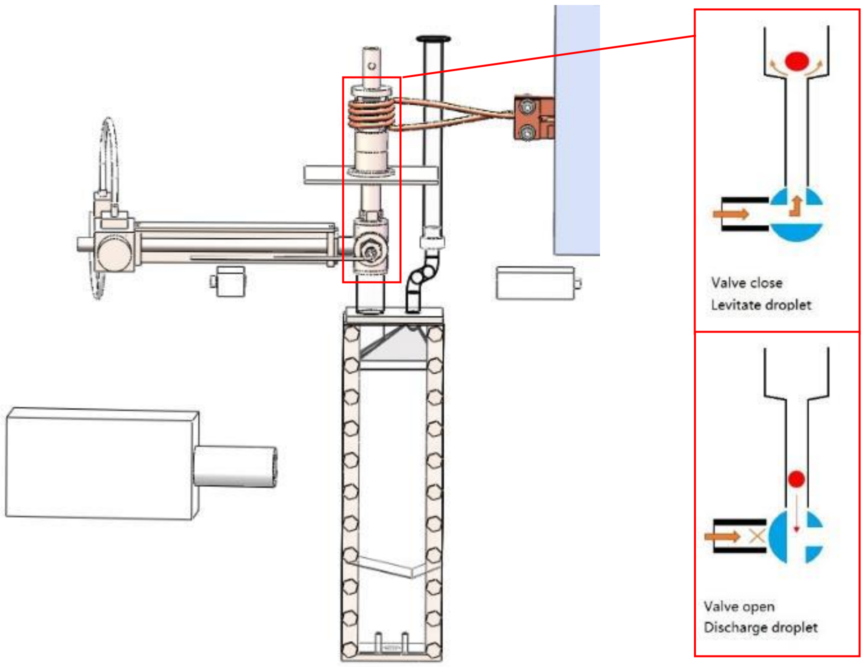

Figure 10: Schematic of the MISTEE facility for Zr/Fe oxidation tests.

To perform oxidation experiments of zircaloy and steel, the MISTEE facility (Manickam et al., 2019a and 2019b) was upgraded to a high operational temperature with installation of appropriate instrumentation. A subsystem was added to physically collect hydrogen which is produced from metallic melt oxidation (Guo et al., 2019b). The hydrogen collecting system consists of a dual nozzle quartz cover, a graduated cylinder and connecting pipes, as shown in Figure 11. The cover was designed to match the tank opening size (150mm×100mm) and the location of the side nozzle was aligned under melt discharging tube. The graduated cylinder (100*ml* with graduation of 1*ml*) fully filled with water prior to experiment is used as a final storage container for rising hydrogen bubbles.

A new furnace with double crucibles (Figure 12) was developed to replace the old furnace with a single crucible previously employed in the MISTEE for molten oxide or Zr droplet tests. The new furnace was motivated by the fact that contamination of carbon was found when the old furnace with graphite crucible was employed to melt Zr-Fe mixture sample, as shown in Figure 13, while it was well-functioning for pure Zr droplet tests. In the double-crucible furnace, the outer crucible was made of graphite to generate heat by induction and the inner crucible was made of refractory materials to minimize sample contamination from the crucible.

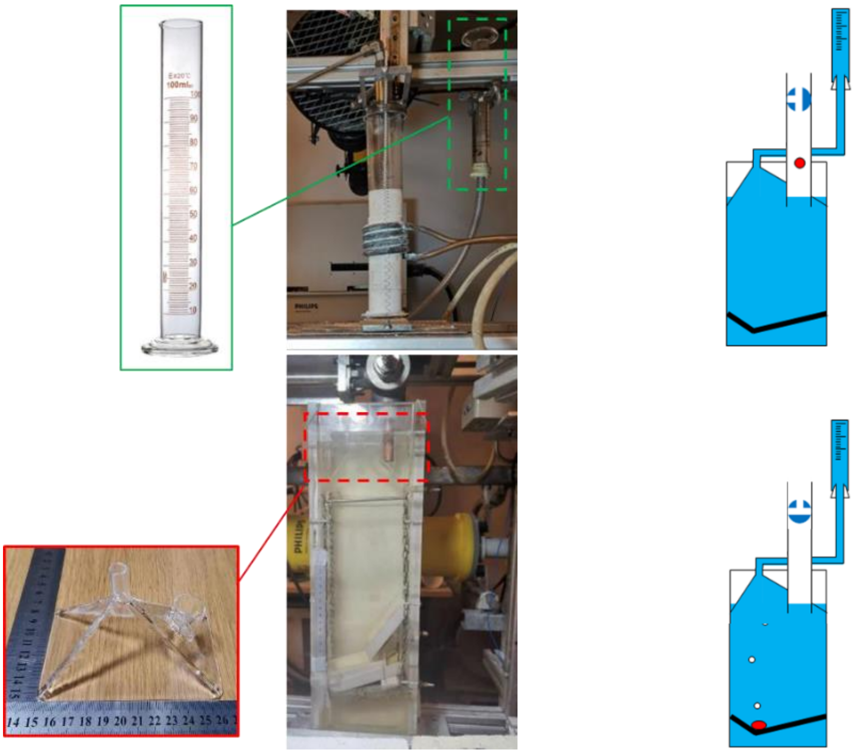

(a) Pictures of main parts (b) Working principle

Figure 11: Schematic of hydrogen collecting system.

For the inner crucible, several high-temperature resistant materials including BN, SiC, Al_2O_3 and MgO, have been testes, and MgO was finally selected since it avoided material interaction between molten Zr-Fe alloy and the crucible. In Figure 14, the SEM results indicated that the elements O and Mg were rarely dissolved in the alloy and the influenced layer of the crucible was within ~10um.

Top view

Front view

Figure 12: Pictures of double crucibles of the new furnace.

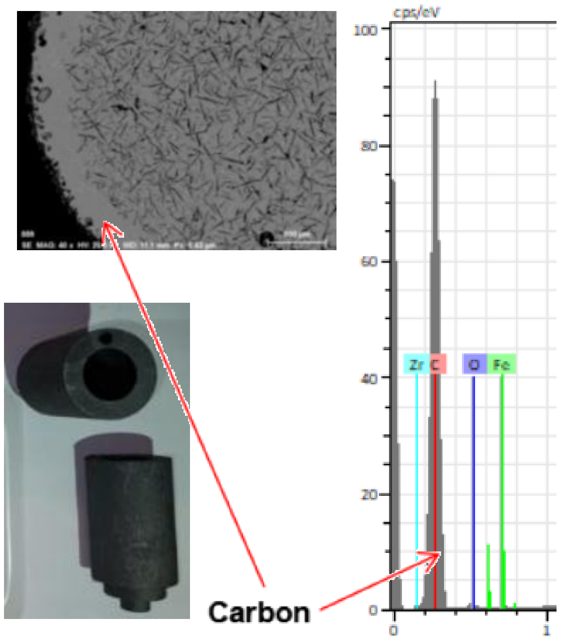

Figure 13: Composition of a refrozen Zr-Fe sample prepared by the old furnace.

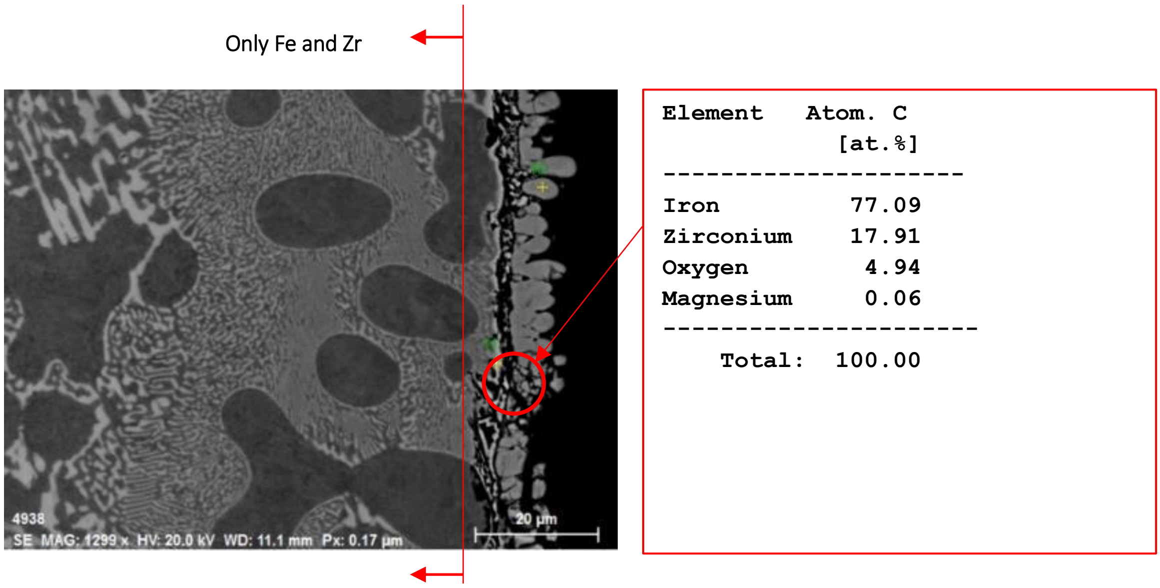

Figure 14: Composition of a refrozen Zr-Fe sample prepared by the new furnace.

To be noted, another meaningful work is the proper preparation of Zr-Fe mixture which can be loaded in the crucible and forming a well-mixed alloy. Three methods had been tested to prepare Zr-Fe mixture melt with the desired composition, as shown in Figure 15. It was found that (1) it is complicated to make tablets from Zr and Fe power, since the powder had a high risk to be partially oxidized during mixing, processing and storage, (2) the melting of mixed Zr and Fe pellets tend to melting into inhomogeneous mixture, and (3) the customized alloy with a proper composition of Zr and Fe is the best method to meet the requirement. Figure 15 shows the photo of refrozen sample prepared in the different methods. Also, a composition examination of the customized alloy by SEM confirmed that the measured percentage of Zr and Fe in the alloy ($Zr_{0.72}$-$Fe_{0.28}$) is close to the expected composition ($Zr_{0.75}$-$Fe_{0.25}$), and no other impurity elements were detected except for O and Hf (~0.5%) which are also existent as trace Zr pellets). All the elements were uniformly distributed in the alloy. Figure 16 shows the hydrogen generation from several tests using Zr-Fe alloy droplets. Similar to the previous tests using pure Zr droplets (Manickam et al., 2019a), the water subcooling has a significant effect on oxidation of melt during quenching of the droplets. However. more tests (including repeating ones) are needed to make a solid conclusion. More details can be found in (Guo et al., 2019d).

Methods of preparation of Zr-Fe alloy	***Refrozen sample of Zr-Fe alloy after melting***
Tablets of pre-mixed Zr and Fe powder 	Partially oxidized melt (remains in crucible) 
Mixed Zr and Fe pellets Zr 99.6%  Fe 99.95% 	Melt not well mixed (remains in crucible) 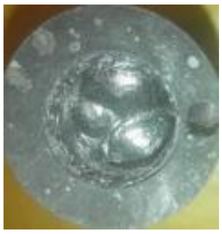
Customized Zr-Fe alloy 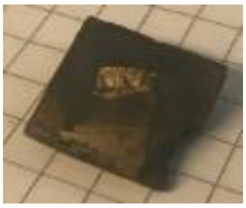	Desired droplets of well-mixed Zr-Fe alloy 

Figure 15: Effects of Zr-Fe alloy preparation on melting.

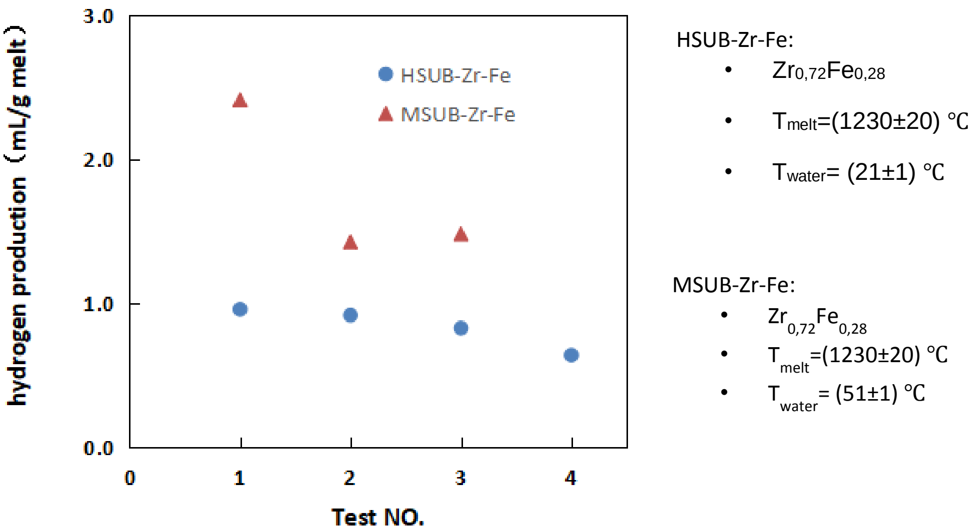

Figure 16: Hydrogen production from oxidation tests using single Zr-Fe droplets.

2.7 Bubble dynamics of film boiling around spheres

During the Fukushima nuclear accidents, raw seawater has been used to cool the reactor cores (IAEA, 2011). After the accidents, attention was paid to the effects of water impurities on core degradation, chemistry and fuel coolant interactions (FCI).

An experimental study was carried out to investigate the effect of seawater on FCI and steam explosion (Guo et al., 2019c), using the MISTEE facility at KTH. Since a steam explosion occurs when the vapor films surrounding the melt droplets collapse, it is important to understand the instability of the vapor films. For this purpose, bubble dynamics of film boiling around a high-temperature sphere during its quenching process was also investigated in the MISTEE platform (Qiang et al., 2018).

The experimental setup (Figure 17) consists of an induction furnace and a water tank filled with deionized (DI) water or seawater with low salinity (the Baltic seawater salinity typical as 7g/kg~8g/kg; Feistel et al., 2010). A 15mm stainless-steel sphere was heated to a prescribed temperature in the induction furnace protected by Argon atmosphere,e and inserted into a transparent water tank. The dynamics of the vapor film during the quenching process was recorded by a high-speed camera, and the sphere's temperature history was acquired by the thermocouple A located in the center of the sphere. The sheath of the thermocouple serves as the holding of the sphere in the water pool. Thermocouple B servers as a reference to help determine the time when the ball enters the water. Thermocouple C is used to monitor the coolant temperature.

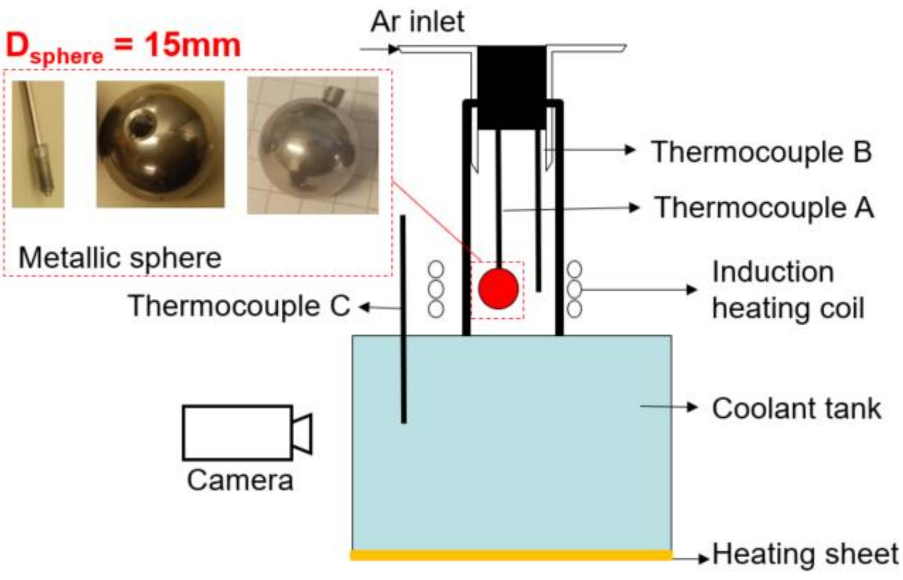

Figure 17: Quenching of stainless-steel sphere in the MISTEE facility.

Figure 18 shows a typical temperature history recorded by Thermocouple A at the center of the sphere when a heated sphere at 1000 °C was immersed in subcooled seawater (40 °C). The figure indicates the stages of the quenching process: vapor film formation, unstable film boiling, stable film boiling, transition boiling, nucleate boiling and natural convection. Upon insertion of the hot sphere into the coolant, a vapor film forms with violent oscillation. Afterwards the vapor film gradually become stable. With decreasing temperature of the sphere, the vapor film will collapse somewhere, leading to direct contact of the sphere with coolant, The transition boiling is finally transferred to nucleate boiling, and then natural convection without further bubble generation. Figure 19 shows the snapshot and time scale of each stage.

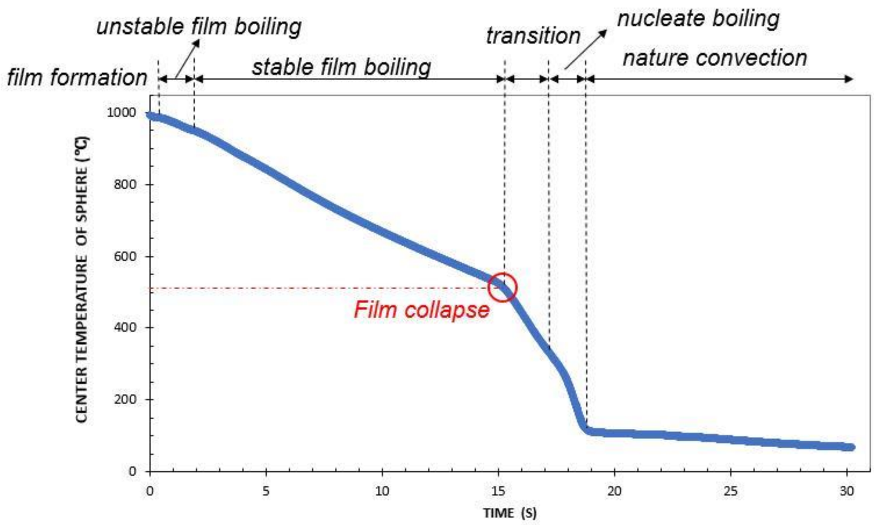

Figure 18: A typical temperature history at the center of the sphere.

Figure 19. Typical stages during quenching of the sphere in coolant.

During quench process of the sphere, the mode of vapor film collapse was observed to be different for DI water and seawater. As shown in Figure 20, the two sequences of pictures illustrate the two different modes of film collapse under the same test condition (the initial temperatures of the sphere and the coolant are 1000℃ and is 40℃, respectively). The vapor film of mode A was translucent within 0.01s after initiating film collapse, and then its transition boiling stage is around 0.04s. For the transition boiling of mode B, a gradual downward receding of vapor film is observed.

After analyzing the film collapse processes of 36 sphere-quench tests (20 runs in seawater and 16 runs in DI water with the same coolant temperature 40℃), it is found that all the film collapse processes in seawater have a similar phenomenon to the mode B, while there is a 44% chance to show the mode A for the spheres quenched in DI water.

In Figure 21 the critical temperature is the temperature at the center of the sphere when the onset of film collapse was observed. And the film collapse time is the time from the onset of the film collapse to the end of transition boiling. As shown in Figure 21, the film collapse time in seawater (SW) is longer than that in DI water (FW). This critical temperature in seawater is higher than DI water, and the critical temperature is higher when vapor film has a collapse mode B.

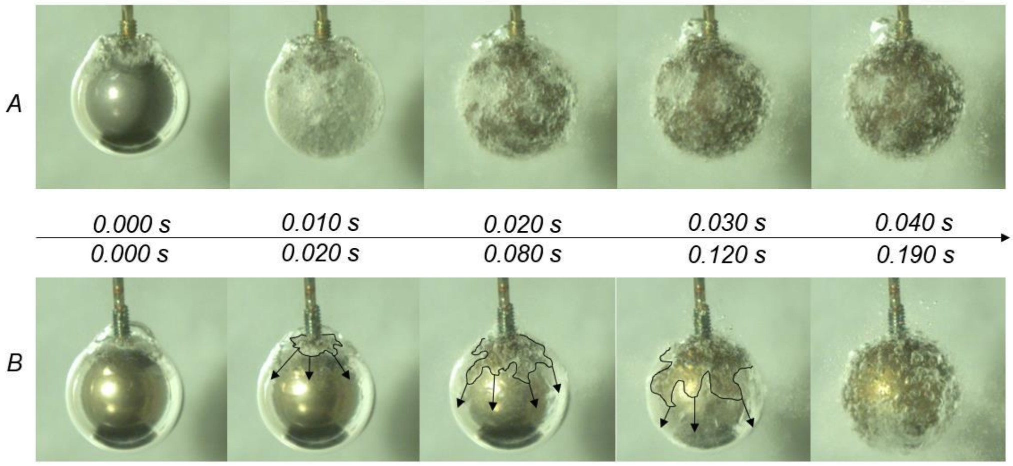

Figure 20: Two modes of film collapse.

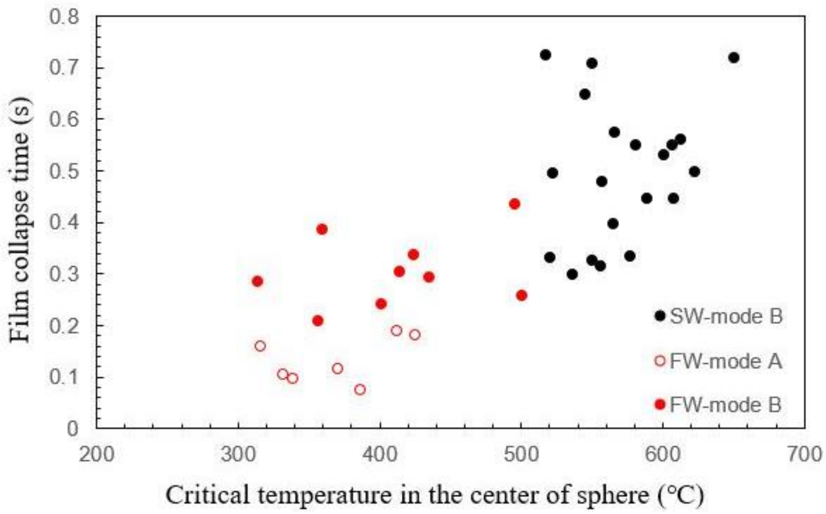

Figure 21: The statistical results for the film collapse time and the critical temperature.

2.8 Analysis of the Fukushima accident using the MELCOR code at VTT

There are still considerable uncertainties associated with severe accident phenomena. This is because of the variety of the phenomena, challenging circumstances and the number of possible scenarios. The Fukushima accident provides a unique opportunity for obtaining more information about the progress and mitigation of severe accidents in Boiling Water Reactors (BWR). Gaining better understanding of the events is essential in evaluating the applied Severe Accident Management (SAM) strategies also in Nordic BWRs.

Developing a calculation model is an excellent way of gaining a deeper understanding of the events at Fukushima and improve modelling practices. Getting insights into the capabilities and weaknesses of the MELCOR code is also an important objective of the work. Analyzing the accidents was started already in 2012, and since then, models of the three units have been continuously developed further when new information has become available. More details can be found in (Deng et al., 2019).

2.8.1 Updating the unit 2 MELCOR model

In 2019, the third version of VTT's MELCOR model of the Fukushima unit 2 accident was developed (Sevón, 2019). Detailed plant data, obtained from the OECD BSAF-2 project, was utilized to eliminate most of the uncertainties that were related to unknown dimensions of the plant. The main new feature in the third version is the reactor water level measurement system (Figure 22). It was based on measuring the pressure difference between two water-filled pipelines (variable leg and reference leg) that were connected to the reactor at different elevations. Adding the measurement system to the MELCOR model makes it possible to analyze the erroneous water level readings that were caused by boiling of the water in the system during the accident.

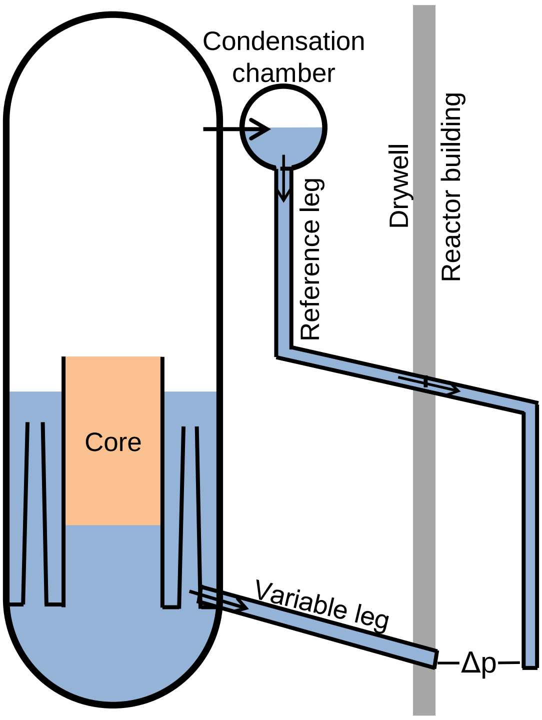

Figure 22. The reactor water level measurement system (Sevón, 2020).

2.8.2 Results

The calculated reactor pressure is compared with the measurements in Figure 23. The good match during the RCIC (Reactor Core Isolation Cooling) operation was achieved by careful manual tuning of the flow rates. The operators depressurized the reactor by opening a Safety Relief Valve (SRV) at 75 h. The calculation model reproduces the depressurization rate and the three pressure peaks at around 80 h quite well.

Figure 24 shows a comparison between the indicated reactor water level, as calculated with the MELCOR model of the measurement system, compared with the raw measurement data. The measurements indicated a sudden recovery of the water level at 78.5 h, and then a stabilization at approximately middle of the core for several days. It is virtually certain that the measurements after 78.5 h did not indicate the actual water level in the reactor and that the distortion was caused by evaporation of the water in the reference and variable legs of the measurement system (Figure 22).

The simulated water level indication agrees with the measurements because a leak of superheated steam from the SRV gasket to the drywell was assumed, starting at 78.5 h. The leaking gas heated up the drywell, causing the water in the measurement system to evaporate. The leak was probably quite small; 8 cm^2 resulted in the best agreement with the measurements. The leak was probably located close to the water level measurement system, so that it caused localized heating of the drywell. The new calculation supports the leak hypothesis that was presented by a Japanese accident investigation committee (ICANPS, 2012).

The Fukushima accident demonstrated that BWR water level measurement systems, which are based on measuring the pressure difference between two water-filled pipelines, can be distorted by temperature changes. The reliability of the measurement systems could be increased by installing thermal insulation around the reference leg and variable leg in the drywell. (Sevón, 2020).

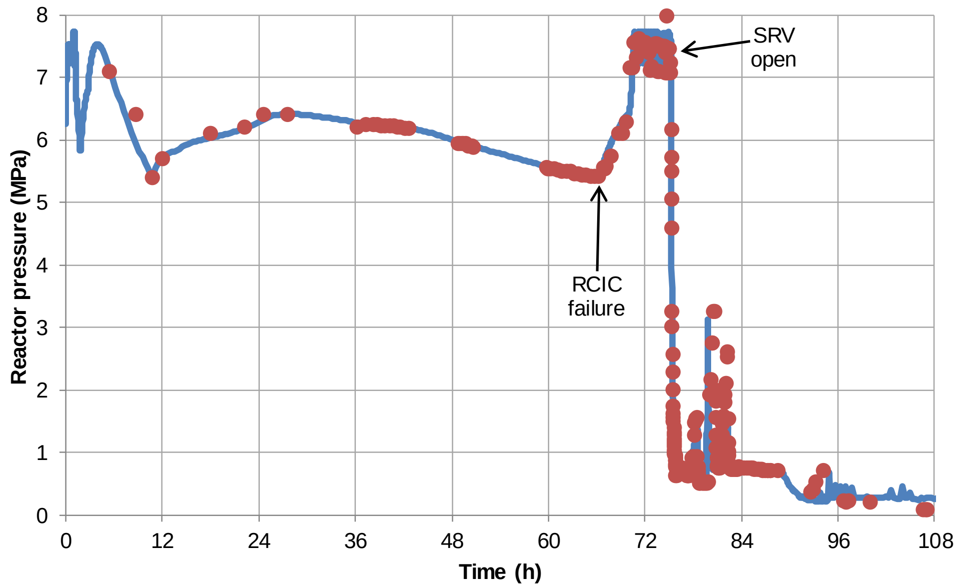

Figure 23: Reactor pressure during the Fukushima unit 2 accident, calculation (blue line) compared with measurements (red circles).

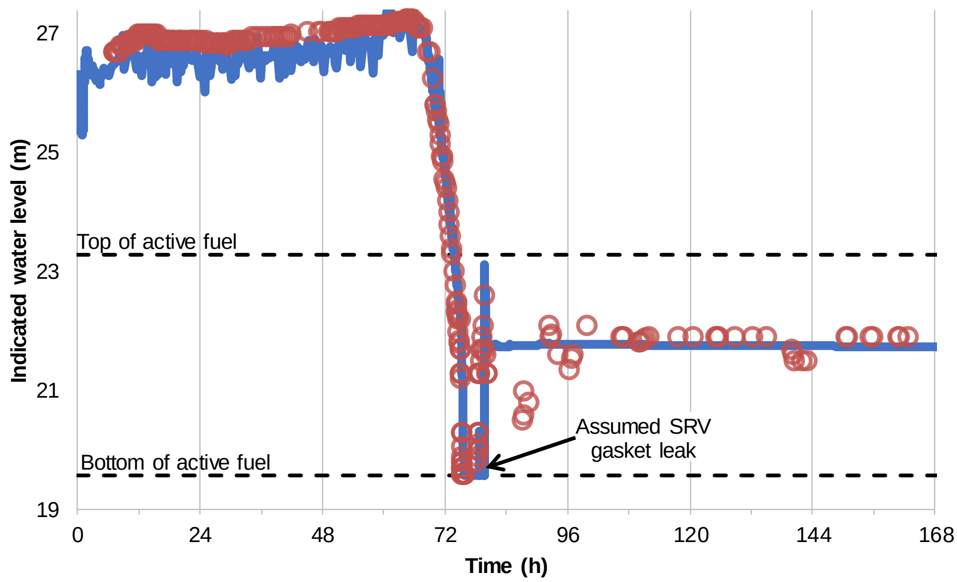

Figure 24: Indicated water level in the reactor, calculated with the simulated water level measurement system, compared with raw measurement data.

Figure 25 shows a comparison between the calculated and measured containment pressure. The dashed green line shows a calculation without the SRV gasket leak. Without the leak the containment pressure would have remained much lower.

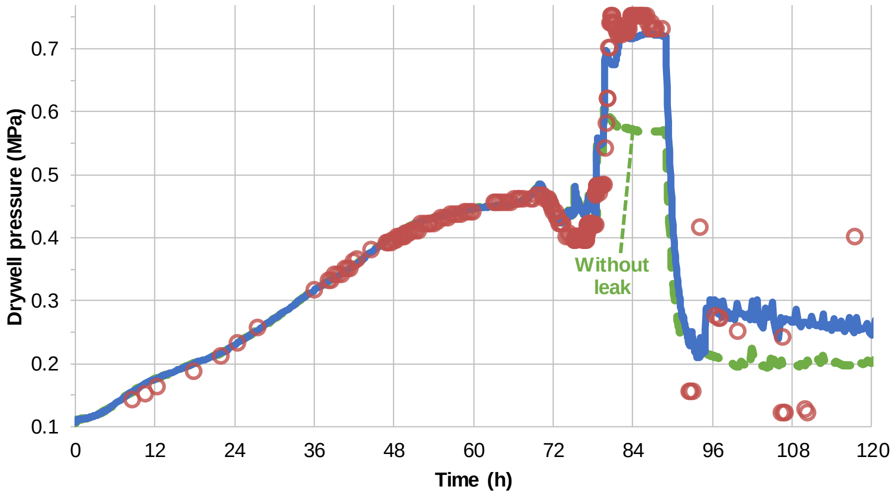

Figure 25: Drywell pressure, calculation compared with measurements. The green dashed line shows a MELCOR calculation without the SRV gasket leak.

2.8.3 Cesium release

The calculated release of cesium from unit 2 to the environment was 2.1 % of the core inventory. In the calculation without the SRV gasket leak, the cesium release was only 0.5 % of the core inventory. The gasket leak increased the release mainly because the aerosols leaked from the reactor to the drywell, bypassing the suppression pool.

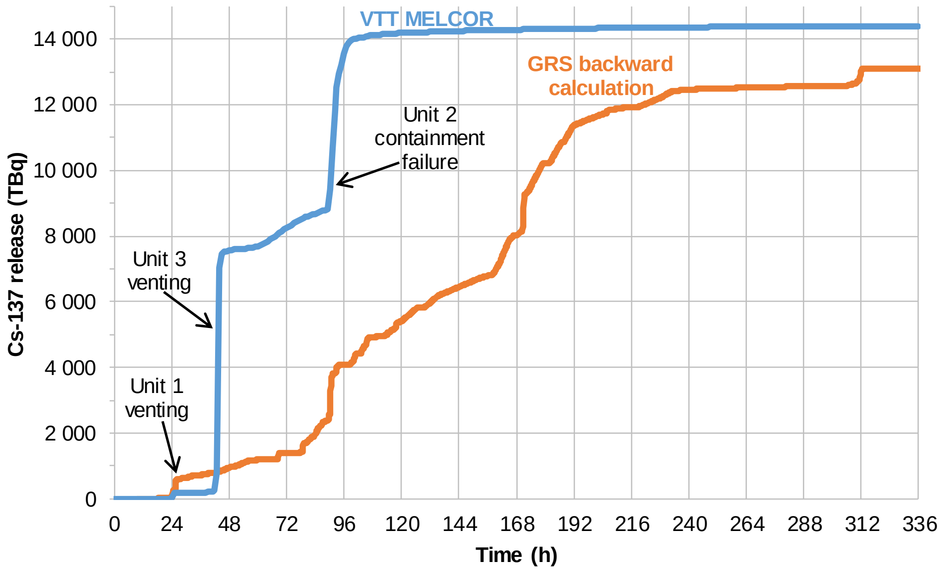

Figure 26: Release of Cs-137 to the environment from all three accident units at Fukushima. VTT's MELCOR calculations, compared with the GRS "backward" calculation that is based on radiation measurements and the local weather (Sogalla et al. 2019).

VTT has developed MELCOR models of all three accident units at Fukushima. Figure 26 shows the total Cs-137 release from all the three units. For comparison, the figure shows a so-called "backward" calculation, performed by Sogalla (2019) based on the measurements in the environment and the local weather data. VTT's current estimate of the total Cs-137 release from all three units is 14.3 PBq (Sevón, 2020). This compares well with the GRS backward calculation (13.1 PBq). However, the time evolution of the release is somewhat different: the MELCOR calculations give two very large release peaks, caused by the unit 3 venting and unit 2 drywell failure, while the environmental measurements hint at steadier releases that continued for a longer time. The unit 3 venting is not visible in the backward calculation because the wind was blowing to the sea, and the land-based measurements could not detect the release.

2.9 CFD analyses of heat transfer in a melt pool at VTT

The most important objective in SAM is to stabilize the core melt. This can be done either in- or ex-vessel. In-Vessel Melt Retention (IVMR) is normally introduced in low-power reactors, where efficient cavity flooding is possible. To new reactor designs has typically been implemented a core catcher: an additional structure between the Reactor Pressure Vessel (RPV) and containment where the core melt should be stabilized. Especially in a crucible type core catcher the melt pool behavior and heat transfer phenomena are very similar to IVMR application. To have an in-depth understanding of these complex phenomena is mandatory to assess if core melt stabilization is successful.

The objective of this work (Ojalehto, 2020) was to create an OpenFOAM-6 (Open Source Field Operation And Manipulation) CFD model to study the melt pool behavior and heat transfer in a volumetrically heated hemispherical pool. In practice, this is done by simulating a SIMECO-2 experiment and benchmarking the results against the pre-test analysis conducted by Li (2016). The results should show the distribution of heat flux on the wall, and additionally e.g. the crust thickness and the flow field.

2.9.1 Experimental facility

The purpose of KTH's SIMECO-2 facility (Figure 27; Komlev et al., 2019 & 2020) is to study the behavior of a 2- and 3-layered stratified melt pool by using simulant materials. The phenomena of interest include the layer inversion, crust formation, the focusing effect as a function of top metallic layer thickness, and heat transfer distribution between the melt pool, wall and the top metal layer.

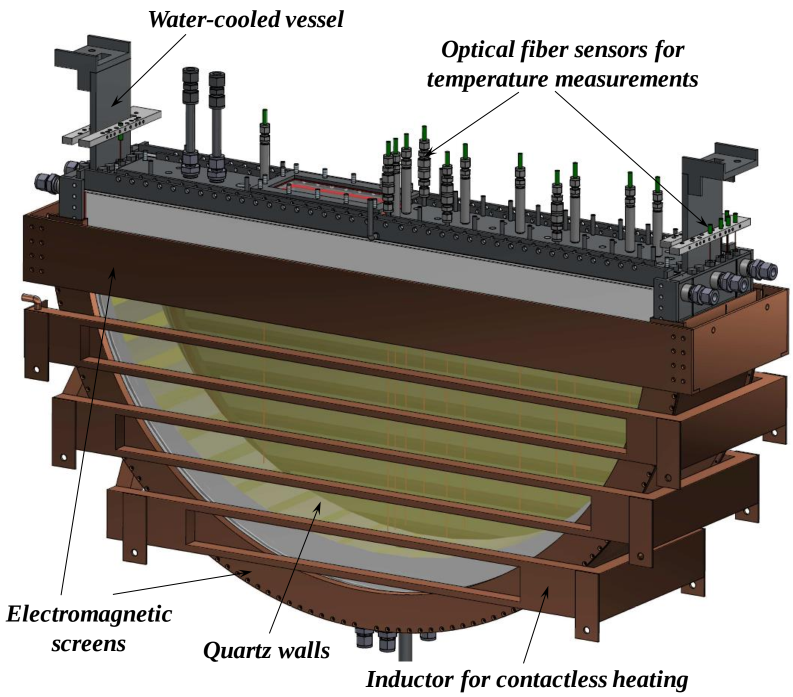

Figure 27: An illustration of the SIMECO-2 test section (Komlev et al., 2019 & 2020).

The semicircular, slice-like test section represents the lower head of a RPV, and it includes a curved steel wall, transparent quartz windows at the sides, and a lid with a window. The simulant is heated contactless by induction. The vessel has a radius of 500 mm and a thickness of 90 mm. According to the latest information, the simulant materials for the oxide and metal layers are CsCl-KCl-LiCl and Al-Mg respectively. The pre-test analysis (Li, 2016), used a different simulant materials for the salt layer, although the exact composition was not mentioned in the work. However, the material properties were given, and for consistency those are used in this work as well.

2.9.2 Characteristics of the model

As the velocities inside the domain are expected to be relatively small, it can be assumed, based on Mach number, that the effect of pressure on the density is negligible, and the flow can be considered incompressible (Kundu and Cohen, 2008). However, this does not rule out the temperature-induced density changes. As most of the large temperature changes occur in a relatively small volume in the solid crust, the effect of these density changes to the flow field were estimated to be negligible.

Additionally, the temperature difference in the liquid region is only ca. 180 K, of which the largest gradient can be found in a small volume near the top surface. The effect of these density changes on the system were estimated small as well. Thus, the density was assumed independent from both the pressure and the temperature and was set as constant.

Setting density constant creates a conflict with the buoyancy effects, as buoyancy is driven by density differences caused by the temperature field. A workaround is to apply Boussinesq approximation in the calculations.

The flow field in the homogeneous melt pool is known to consist of both turbulent and laminar regions. The flow in the near-wall regions shows some turbulent behavior, whereas the slow upwards flow in the middle could be considered laminar. Turbulence affects both the flow field and the heat transfer in the system, so it was included in the calculations.

The solidification model implemented in the model is based on a fixed-grid enthalpy method introduced by Voller and Prakash (Voller and Prakash, 1987). The model assumes a non-isothermal phase change, i.e. phase change occurs between two temperatures: solidus temperature and liquidus temperature. Below the solidus temperature, the fluid is assumed completely solid, and above the liquidus temperature, it is completely liquid. In between lies the so-called mushy region that consists of both the solid and the liquid phases at the same time.

The model is kept very simple, and thus the solidifying process is not modelled in detail, i.e. there is no particle tracking, crystallization or volume contraction. Instead, the solidification is simulated by assuming zero fluid velocity at certain temperature and liquid fraction. This is done by adding a momentum sink in the momentum equation. The mushy region is modelled as a pseudo-porous zone, in which the properties are defined by the liquid fraction. The liquid fraction is defined by temperature and latent heat (Voller and Prakash, 1987).

Custom polynomial models were used to set different temperature dependent material properties for the liquid and solid regions as presented in Table 3 and interpolate the values for the mushy region.

Table 3: Physical properties of the working fluid

Property	Temperature range, K	Expression
Solidus temperature (T_{sol}), K	-	923
Liquidus temperature (T_{liq}), K	-	983
Density, kg·m^{-3}	$\geq T_{liq}$	2678.5
	$\leq T_{sol}$	
Dynamic viscosity, mPa·s	$\geq T_{liq}$	$0.00003493 \cdot T^2 - 0.087463 \cdot T + 57$
	$\leq T_{sol}$	
Thermal conductivity, W·m^{-1}·K^{-1}	$\geq T_{liq}$	$0.519 - 0.000131338 \cdot T$
	$\leq T_{sol}$	$4.00 - 0.002822 \cdot T$
Heat capacity, J·kg^{-1}·K^{-1}	$\geq T_{liq}$	663.29
	$\leq T_{sol}$	$424.66 + 0.146818616 \cdot T$
Heat of fusion, J·kg^{-1}	$=T_{sol}$	203 526
Emissivity	$\geq T_{liq}$	0.5
	$\leq T_{sol}$	
Thermal expansion coefficient, 1/K	$\geq T_{liq}$	$4.17 \cdot 10^4$
	$\leq T_{sol}$	

2.9.3 Mesh and boundary conditions

The shape of the SIMECO-2 test section is a semicircular slice. The vessel and the phenomena within were assumed symmetrical, so only a quarter of the vessel was considered. A screenshot of the mesh is shown in Figure 28. The radius of the domain is 0.5 m and the width is 0.045 m. There are in total 30 020 cells in this rather coarse mesh. To study the effect of nodalization, the case is also run with a finer mesh having up to 90 000 cells.

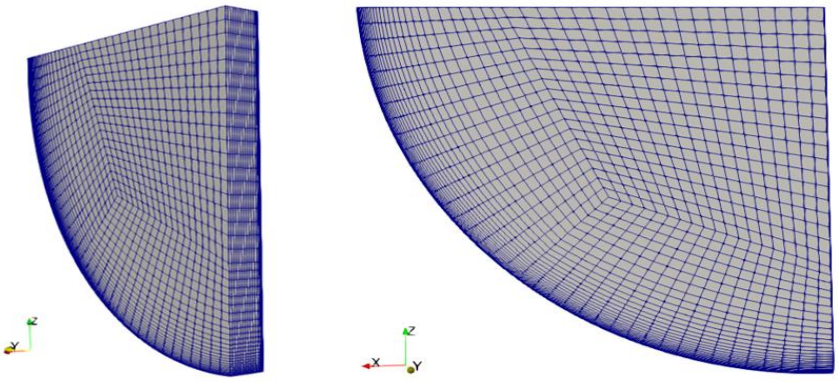

Figure 28: The mesh in 3D (left) and in 2D (right).

Due to the solidification, the model does not really benefit from the small cell sizes near the curved wall. Instead, the small cells should be placed on the crust surface. The mesh was thus refined around the mushy zone and the higher velocity region.

The top surface of the melt pool was modelled as a free, adiabatic surface. The side in contact with the quartz walls was modelled as adiabatic wall. The steel wall next to the curvature was taken into account by setting a boundary condition including external heat transfer coefficient and ambient temperature that were set constant along the curvature. Constant external wall temperature (Ta = 343 K) was achieved by setting the external heat transfer coefficient to a very large value. To model the conduction through the steel layer, also the thickness of the vessel wall (0.015 m) and the thermal conductivity of steel (20 W/mK) were defined.

The pool temperature was set to 1 073 K in the beginning of the simulation. This means that the pool was considered completely liquid. Volumetric heat generation in the pool was 0.5 MW/m3. The model was run for 3 000 seconds until the system reached a steady state.

2.9.4 Results

The results obtained from the OpenFOAM simulations with the rather coarse mesh were compared with the results from the pre-test analysis. The most important phenomena to compare were the temperature distribution in the pool, the crust thickness, the heat flux on the wall, and the heat transfer in the pool. Additionally, the computed flow field is also presented.

The velocity streamlines are illustrated in Figure 29. The figure show that there is natural convection occurring in the pool. In the middle, the hotter liquid rises slowly upwards, whereas in the colder region near the crust interface the downward flow is relatively fast. There also seems to be some instability in the upper region, which is most likely caused by the mesh. The cells in the problematic region are not aligned with the flow field, which could induce a phenomenon called numerical or false diffusion (Versteeg and Malalasekera, 2007).

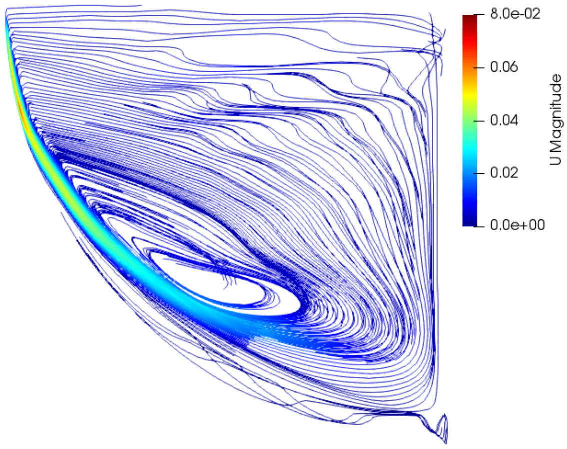

Figure 29: Velocity streamlines.

In the pre-test analysis, it was mentioned that the order of the magnitude of the flow velocity was ca. $10^{-2}\ m/s$. As the above figures show, the velocities in the system seem to agree with the previous statement.

The temperature distribution in the pool is shown in Figure 30 below. It can be seen that the temperature stratifies into different layers from the cold bottom to the hotter top region. A colder region can also be observed near the steel wall. The temperature range in the pool was 361 K – 1155 K. The temperature distribution on a vertical centerline is shown in

Figure 31 with the corresponding values from the pre-test analysis.

As

Figure 31 shows, there seem to be some deviation in the centerline temperatures. In the pre-test analysis, the temperatures at the upper parts of the pool are higher, the maximum temperature difference between the two cases being approximately 100 K. The most probable reason for this is the lower mesh density. It was shown in the mesh sensitivity study, that the mesh density has a significant effect on both the wall heat flux and the surface temperature. The temperature deviation might also have an effect on the crust thickness that is shown in Figure 32.

The crust thicknesses and shapes seem to differ between the two works. In the pre-test analysis, the mushy-solid region seems to be significantly narrower. However, the depth of the fully liquid pool is approximately the same. Differences in the mushy zone are probably caused by the differences in the solidification model.

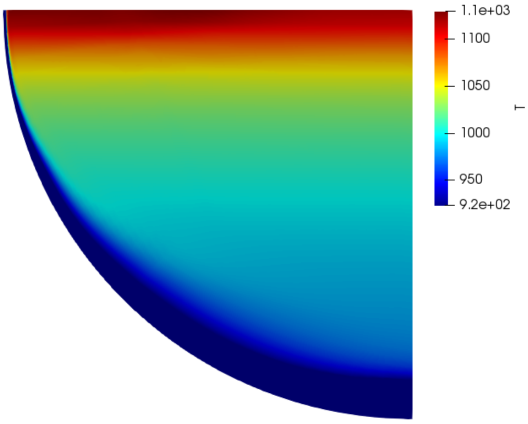

Figure 30: Temperature distribution in the pool.

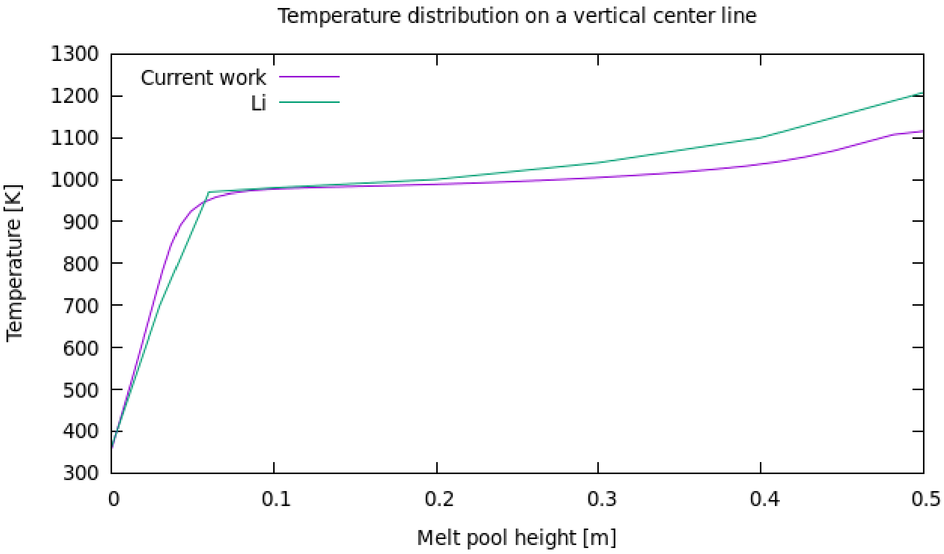

Figure 31: A comparison of the temperature distributions on a vertical centerline.

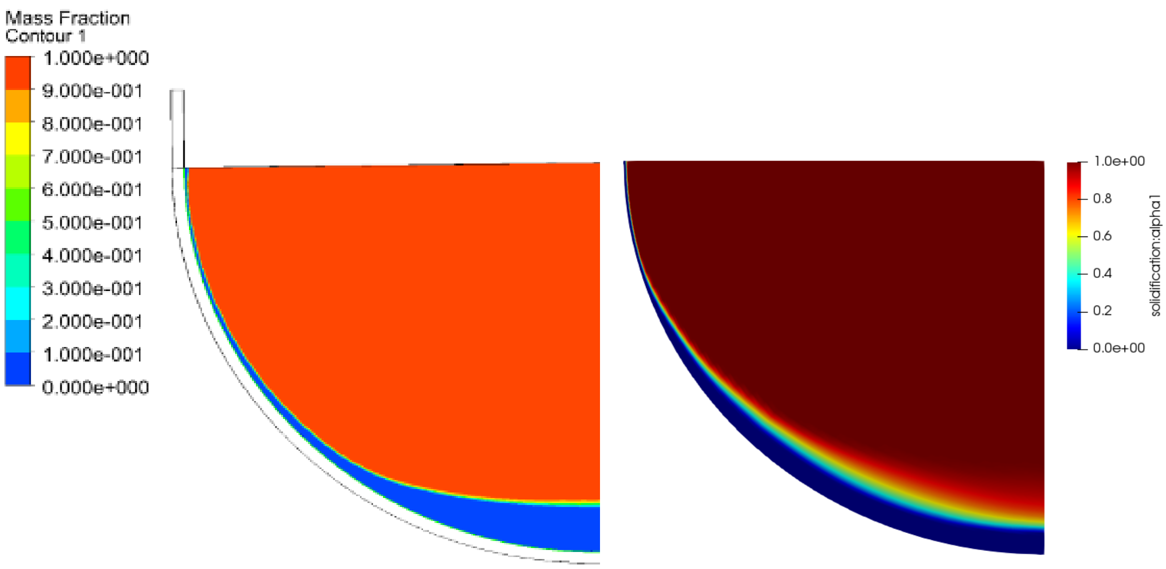

Figure 32: Comparison of the crust thicknesses. Left: data from the pre-test analysis (Li, 2016), cropped for consistency, and right: this work.

Another important parameter to compare is the distribution of the heat flux on the wall. Figure 33 shows the distributions of the local wall heat fluxes as a function of the pool angle. The results are in a good agreement.

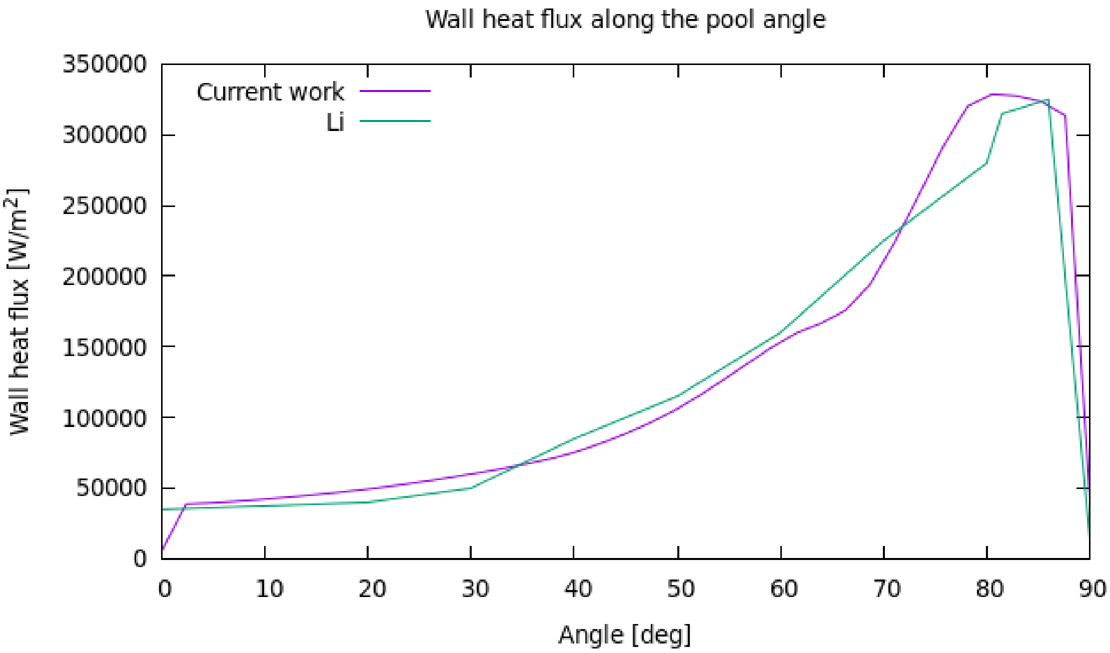

Figure 33: The local wall heat flux along the pool angle.

3. Concluding Remarks

Significant progress was made and important findings were obtained in the SPARC project carried out by KTH and VTT during 2019. The focus of this project is to produce new data and to develop models and methodologies for addressing severe accident scenarios and phenomena which are important to assess the risk of containment failure and radioactivity release in postulated severe accidents of Nordic NPPs. The main achievements obtained are as follows.

At KTH, the development of the SIMECO-2 facility is at the final stage before completion, which is intended to address the behavior of core melt (corium) in the lower head of a light water reactor (LWR) during postulated severe accidents, including heat and mass transfer in a molten pool of oxidic and metallic corium simulants, as well as remelting of debris bed and molten pool formation. Meanwhile, more pre-test simulations were performed at both KTH and VTT.

A surrogate model for quick estimate of debris bed coolability was developed at KTH to predict the dryout power density of multi-dimensional debris bed based on the database calculated by the COCOMO code (full model). The surrogate model is successfully developed with Kriging method, and the validation demonstrates that the deviation from the full model is within 10%. The surrogate model was employed to generate the coolability maps regarding the variation of porosity and particle size of prototypical debris beds postulated in ex-vessel debris scenarios of a reference Nordic BWR.

To fill in the knowledge gap of fuel coolant interactions during the first pour of melt upon vessel failure, metallic melt was employed in the DEFOR-M experiment at KTH. The experimental results show that the melt jet breakup length is closely estimated by the Saito correlation and lies between those of Taylor correlation and Matsuo correlation. Larger debris particles dominate in low superheat cases while smaller particles were obtained in high superheat cases. High melt superheat and low subcooling cause a significant amount of agglomeration and cake formation. High water subcooling and low melt superheat led the formation of more porous debris bed, with different particle morphology and particle size distribution.

A parametric code named transIVR was developed at KTH for the transient melt pool heat transfer analysis. It is mainly based on limped-parameter estimate of heat transfer in melt pool using empirical correlations, as well as resolution of 2D heat conduction in the RPV wall with finite difference method. The code was further coupled with the ANSYS Mechanical code for RPV failure analysis. Validations of the transIVR code against the UCSB FIBS benchmark case and the LIVE-7V experiment show the capabilities of the code for predicting both steady-state and transient heat transfer of melt pools. The calculation of the FOREVER-EC2 experiment using the code coupled with ANSYS Mechanical demonstrates the efficiency of RPV failure analysis with reasonable accuracies in terms of failure location and timing.

The MISTEE facility at KTH was upgraded to perform oxidation experiment of molten Zr-Fe alloy droplets: a subsystem was added to collect hydrogen, and a new furnace with double crucibles was developed for preparation of Zr-Fe droplets to avoid material interaction between melt and crucible. Preliminary results show a significant effect of water on oxidation of the melt droplet during its quenching in the water pool. The effect of seawater on film boiling was also investigated through quenching process of a hot stainless-steel sphere in the MISTEE facility. The critical temperature for the onset of film collapse in seawater is higher than that DI water. The film collapse time in seawater is also longer than that in DI water. Two different modes of vapor film collapse were observed: only mode A in seawater and both modes in DI water.

At VTT, the third version of VTT's MELCOR model of the Fukushima unit 2 accident was developed. This included adding a model of the reactor water level measurement system to analyze the erroneous water level readings. The calculation reproduces the measured reactor and containment pressures well. This required manual tuning of the RCIC flow rates and the flooding rate of the torus room.

Most of the remaining uncertainties are related to physical and chemical models and nodalization in MELCOR and uncertain boundary conditions. The locations, sizes and timings of leaks from the reactor to the containment and from the containment to the reactor building are still uncertain, as well as the water injection rate with the fire engine.

An OpenFOAM-6 CFD model was created for SIMECO-2 experiment to study the melt pool behavior and heat transfer in a volumetrically heated hemispherical pool. Temperature distribution in the pool, crust thickness and heat flux on the wall were compared with a pre-test analysis at KTH. The results seemed to agree reasonably with the rather coarse mesh. Results with the finer mesh are still under evaluation.

References

Abe, Y., Kizu, T., Arai, T., Nariai, H., Chitose, K., Koyama, K., 2004. Study on thermal-hydraulic behavior during molten material and coolant interaction. *Nuclear Engineering and Design* 230, 277–291.

Bian, B.,Villanueva, Bechta, S., 2019. Direct Numerical Simulation of SIMECO-2 experiment. Proceeding of the 49th MSWI Meeting, Stockholm, December 11.

Chen, Y., Ma, W., 2019. Development of surrogate model for debris bed coolability analysis. Proceedings of the 18th International Topical Meeting on Nuclear Reactor Thermal Hydraulics (NURETH-18), Portland, USA, August 18-22.

Deng, Y., Guo, Q., Ma, W., Bechta, S., 2019. Bubble dynamics of film boiling around spheres. Proceeding of the 49th MSWI Meeting, Stockholm, December 11.

Esmaili, H., Khatib-Rahbar, M., Basu, S., 2004. Analysis of In-vessel retention and ex-vessel fuel coolant interaction for AP1000. NUREG/CR-6849, ERI/NRC 04-201.

Feistel, R., Weinreben, S., Wolf, H., Seitz, S., Spitzer, P., Adel, B., Nausch, G., Schneider, B., Wright, D.G., 2010. Density and absolute salinity of the baltic sea 2006-2009. Ocean Science. https://doi.org/10.5194/os-6-3-2010.

Guo, Q., Manickam, L., Ma, W., Bechta, S., 2018. Investigation on quenching of a high-temperature spherical particle in sea water, Proc. of the 12th International Topical Meeting on Nuclear Thermal-Hydraulics, Operation and Safety, Qingdao, China, October 14-18.

Guo, Q., Manickam, L., Yu, P., Villanueva, W., Ma, W., 2019a. A design study on an aerodynamic levitation system for droplet preparation in steam explosion experiment. Proceedings of the 27th International Conference on Nuclear Engineering. (ICONE-27), Tsukuba, Ibaraki, Japan, May 19-24.

Guo, Q., Manickam, L., Komlev, A., Ma, W., Bechta, S., 2019b. On oxidation of a zirconium droplet falling in subcooled water. Proceedings of SWINTH-2019, Paper number 039, Livorno, Italy, Oct. 22-25.

Guo, Q., Manickam, L., Ma, W., Bechta, S., 2019c. Effects of salinity in coolant on steam explosion, in: 18th International Topical Meeting on Nuclear Reactor Thermal Hydraulics, NURETH 2019 : American Nuclear Society, pp. 4556–4567.

Guo, Q., Deng, Y., Ma, W., Bechta, S., 2019d. MISTEE experiment on oxidation of metallic droplets. Proceeding of the 49th MSWI Meeting, Stockholm, December 11.

Huang, Z., Ma, W., 2019. On the quench of a debris bed in the lower head of a Nordic BWR by coolant injection through control rod guide tubes. *Nuclear Engineering and Design* 351: 189–202.

Huang, Z., 2019. Numerical Investigations on Debris Bed Coolability and Mitigation Measures in Nordic Boiling Water Reactors. Doctoral Dissertation, Royal Institute of Technology, Stockholm.

Huang, Z., Ma, W., 2018a. Validation and application of the MEWA code to analysis of debris bed coolability. *Nuclear Engineering and Design* 327: 22–37.

Huang, Z., Ma, W., 2018b. Numerical investigation on quench of an ex-vessel debris bed at prototypical scale. *Annals of Nuclear Energy* 122: 47–61.

Hotta, A., Akiba, M., Morita, A., Konovalenko, A., Villanueva, W., Bechta, S., et al., 2019. Experimental and analytical investigation of formation and cooling phenomena in high temperature debris bed, *Journal of Nuclear Science and Technology* 57: 353-369.

Hoseyni, S.M., Thakre, S., Villanueva, W., Komlev, A., Sköld, P., Bechta, S., 2019a. Investigation of melt flow in porous media: recent experiments. Proceeding of the 48th MSWI Meeting, Stockholm, June 4.

Hoseyni, S.M., Villanueva, W., Komlev, A., Thakre, S., Sköld, P., Bechta, S., 2019b. Current status of MRSPOD experiments: melt infiltration through porous media with solidification. Proceeding of the 49th MSWI Meeting, Stockholm, December 11.

IAEA, 2011. Fukushima Nuclear Accident Update Log. International atomic energy agency. https://doi.org/10.1186/s12939-016-0469-7.

ICANPS, 2012. Final report. Investigation Committee on the Accident at the Fukushima Nuclear Power Stations of Tokyo Electric Power Company.

Karbojian, A., Ma, W.M., Kudinov, P., Dinh, T.N., 2009. A scoping study of debris bed formation in the DEFOR test facility. *Nuclear Engineering and Desig*n 239: 1653-1659.

Komlev, A., Villanueva, W., Konovalenko, A., Peng, Y., Khan, M., Sköld, P., Harti, M., Laato, T., Ma, W., Bechta, S., 2019. Final report on top cooling. Deliverable D3.11 of the EU project IVMR.

Komlev, A., Villanueva, W., Konovalenko, A., Khan, M., Sköld, P., Ma, W., Bechta, S., 2020. Future experimental facility for IVR study: SIMECO-2. International Seminar IVMR-2020, Juan-les-Pins, France, January 21-23.

Khan, M., Komlev, A., Andrei Komlev, Villanueva, W., Yu, P., Bechta, S., 2019. Effect of internal radiation on natural convective heat transfer in a volumetrically heated molten pool. Proceeding of the 48th MSWI Meeting, Stockholm, June 4.

Kudinov, P., Karbojian, A., Ma, W., Dinh, T.N., 2010. The DEFOR-S experimental study of debris formation with corium simulant materials, *Nuclear Technology* 170: 219-230.

Kundu, P.K., Cohen, I.M., 2008. Fluid Mechanics, 4th ed. Elsevier.

Li, L., Ma, W., Thakre, S., 2012. An experimental study on pressure drop and dryout heat flux of two-phase flow in packed beds of multi-sized and irregular particles. *Nuclear Engineering and Design* 242: 369–378.

Li, Y., 2016. CFD Pre-test Analysis of SIMECO-2 Experiment. Master Thesis, Royal Institute of Technology, Stockholm.

Ma, W., Dinh, T., 2010. The effects of debris bed’ s prototypical characteristics on corium coolability in a LWR severe accident. *Nuclear Engineering and Design* 240: 598–608.

Madokoro, H., Miassoedov, A., Schulenberg, T., 2018. Assessment of a lower head molten pool analysis module using LIVE experiment. *Nuclear Engineering and Design* 330: 51–58.

Magallon, D., Huhtiniemi, I., Hohmann, H., 1999. Lessons learnt from FARO/TERMOS corium melt quenching experiments. *Nuclear Engineering and Design*, 189: 223-238.

Magallon, D., Huhtiniemi, I., 2001. Corium melt quenching tests at low pressure and subcooling water in FARO, *Nuclear Engineering and Design*, 204: 369-376.

Manickam, L., Guo, Q., Komlev, A., Ma, W., Bechta, S., 2019a. Oxidation of molten zirconium droplets in water. *Nuclear Engineering and Design* 354: 110225.

Manickam, L., Qiang, G., Ma, W., Bechta, S., 2019b. An experimental study on the intense heat transfer and phase change during melt and water interactions. *Experimental Heat Transfer* 32: 251–266.

Miassoedov, A., Gaus-Liu, X., Cron, T., Fluhrer, B., 2014. Live experiments on melt pool heat transfer in the reactor pressure vessel lower head. Presented at the 10th International

Conference on Heat Transfer, Fluid Mechanics and Thermodynamics (HEFAT 2014), Orlando, FL.

Ojalehto, S., 2020. Master’s Thesis: Computational Fluid Dynamics Analysis of Heat Transfer in Nuclear Reactor Core Melt Pool.

Pohlner, G., Vujic, Z., Bürger, M., Lohnert, G., 2006. Simulation of melt jet breakup and debris bed formation in water pools with IKEJET/IKEMIX. *Nuclear Engineering and Design* 23: 2026–2048.

Rempe, J.L., Knudson, D.L., Allison, C.M., Thinnes, G.L., Atwood, C.L., 1997. Potential for AP600 in-vessel retention through ex-vessel flooding (No. INEEL/EXT--97-00779). United States.

Sevón, T., 2020. Analysis of reactor water level measurements during the Fukushima unit 2 accident.

Sevón, T., 2019. Fukushima unit 2 accident modeling with MELCOR, version 3. VTT Technical Research Centre of Finland ((Research report VTT-R-01274-19)).

Sogalla, M., 2019. Reconstruction of the Fukushima source term from nearby radiological measurements, in: 18th International Topical Meeting on Nuclear Reactor Thermal Hydraulics (NURETH-18), Portland, Oregon, August 18–22.

Spencer, B.W., Wang, K., Blomquist, C.A., McUmber, L.M., Schenider, J. P., 1994. Fragmentation and quench behaviour of corium melt streams in water. NUREG/CR-6133, ANL-93/32.

Thakre, S., Li, L., Ma, W., 2014. An experimental study on coolability of a particulate bed with radial stratification or triangular shape. *Nuclear Engineering and Design* 276: 54–63.

Thakre, S., Xiang, Y., Villanueva, W., Komlev, A., Ma, W., Bechta, S., 2019. Fragmentation of metallic melt jet in a water pool. Proceeding of the 49th MSWI Meeting, Stockholm, December 11.

Theerthan, A., Karbojian, A., Sehgal, B.R., 2001. EC-FOREVER experiments on thermal and mechanical behavior of a reactor pressure vessel during a severe accident, Technical report-1: EEC-FOREVER-2 test. Technical Report SAM-ARVI-D008, March.

Theofanous, T.G., Liu, C., Additon, S., Angelini, S., Kymaelaeinen, O., Salmassi, T., 1996. In-vessel coolability and retention of a core melt. Volume 2. Argonne National Lab., DOE/ID--10460-VOL.2.

Theofanous, T.G., Liu, C., Additon, S., Angelini, S., Kymäläinen, O., Salmassi, T., 1997. In-vessel coolability and retention of a core melt. *Nuclear Engineering and Design* 169: 1–48.

Versteeg, H., Malalasekera, W., 2007. An Introductionto Computational Fluid Dynamics, 2nd ed. Pearson Education Limited, Harlow.

Voller, V.R., Prakash, C., 1987. A Fixed Grid Numerical Modelling Methodology for Convection-Diffusion Mushy Region Phase-Change Problems. *International Journal of Heat and Mass Transfer* 30: 1709–1719.

Xiang, Y., Thakre, S., Villanueva, W., Komlev, A., Ma, W., Bechta, S., 2019 Characteristics of metallic debris beds. Proceeding of the 49th MSWI Meeting, Stockholm, December 11.

Yu, P., Ma, W., Villanueva, W., Karbojian, A., Bechta, S., 2019. Validation of a thermo-fluid-structure coupling approach for RPV creep failure analysis against FOREVER-EC2 experiment. *Annals of Nuclear Energy* 133: 637–648.

Yu, P., 2020. Modelling and Simulation of Reactor Pressure Vessel Failure during Severe Accidents. Doctoral Dissertation, Royal Institute of Technology, Stockholm.

Bibliographic Data Sheet **NKS-440**

Title	Scenarios and Phenomena Affecting Risk of Containment Failure and Release Characteristics
Author(s)	Weimin Ma[1], Peng Yu[1], Yangli Chen[1], Sachin Thakre[1], Yan Xiang[1], Qiang Guo[1], Yucheng Deng[1], Andrei Komlev[1], Walter Villanueva[1], Sevostian Bechta[1] Tuomo Sevón[2], Sara Ojalehto[2], Anna Korpinen[2]
Affiliation(s)	[1]Royal Institute of Technology (KTH) [2]Technical Research Centre of Finland Ltd (VTT)
ISBN	978-87-7893-532-8
Date	July 2020
Project	NKS-R / SPARC
No. of pages	35
No. of tables	3
No. of illustrations	33
No. of references	52

Abstract
max. 2000 characters

The objectives of the project "Scenarios and Phenomena Affecting Risk of Containment Failure and Release Characteristics", dubbed SPARC, is to produce new data as well as to develop models and methodologies for addressing severe accident scenarios and phenomena which are important to assess the risk of containment failure and radioactivity release in postulated severe accidents of Nordic nuclear power plants.

In 2019 substantial advances and achievements in experimental and analytical capabilities as well new insights into physical mechanisms were gained at KTH and at VTT for: (i) experimental development and analysis of melt pool heat transfer; (ii) modeling and analysis of ex-vessel debris bed coolability; (iii) experimental study on melt coolant interaction and debris formation using metallic melt; (iv) development of a parametric code for estimating melt pool heat transfer and its application in vessel failure analysis; (v) experimental study on oxidation of metallic droplets; (vi) investigation of the effect of seawater on quenching of a hot sphere; (vii) analysis of the Fukushima accident using the MELCOR code; and (viii) CFD analyses of heat transfer in a melt pool with OpenFOAM.

This report summarizes the main advancements and findings. More

details can be found in the relevant publications as listed in References.

Key words Severe accident, melt pool heat transfer, debris coolability, fuel coolant interaction, MELCOR simulation.

Available on request from the NKS Secretariat, P.O.Box 49, DK-4000 Roskilde, Denmark.
Phone (+45) 4677 4041, e-mail nks@nks.org, www.nks.org